A cell cycle-regulated Slx4–Dpb11 complex promotes the resolution of DNA repair intermediates linked to stalled replication

Dalia Gritenaite,[1,7] Lissa N. Princz,[1,7] Barnabas Szakal,[2] Susanne C.S. Bantele,[1] Lina Wendeler,[1] Sandra Schilbach,[1,6] Bianca H. Habermann,[3] Joao Matos,[4] Michael Lisby,[5] Dana Branzei,[2] and Boris Pfander[1,8]

[1]DNA Replication and Genome Integrity, Max-Planck Institute of Biochemistry, 82152 Martinsried, Germany; [2]Fondazione IFOM, Istituto FIRC di Oncologia Molecolare, 20139 Milan, Italy; [3]Computational Biology, Max-Planck Institute of Biochemistry, 82152 Martinsried, Germany; [4]Institute of Biochemistry, Eidgenössische Technische Hochschule Zürich, 8093 Zürich, Switzerland; [5]Department of Biology, University of Copenhagen, 2200 Copenhagen, Denmark

A key function of the cellular DNA damage response is to facilitate the bypass of replication fork-stalling DNA lesions. Template switch reactions allow such a bypass and involve the formation of DNA joint molecules (JMs) between sister chromatids. These JMs need to be resolved before cell division; however, the regulation of this process is only poorly understood. Here, we identify a regulatory mechanism in yeast that critically controls JM resolution by the Mus81–Mms4 endonuclease. Central to this regulation is a conserved complex comprising the scaffold proteins Dpb11 and Slx4 that is under stringent control. Cell cycle-dependent phosphorylation of Slx4 by Cdk1 promotes the Dpb11–Slx4 interaction, while in mitosis, phosphorylation of Mms4 by Polo-like kinase Cdc5 promotes the additional association of Mus81–Mms4 with the complex, thereby promoting JM resolution. Finally, the DNA damage checkpoint counteracts Mus81–Mms4 binding to the Dpb11–Slx4 complex. Thus, Dpb11–Slx4 integrates several cellular inputs and participates in the temporal program for activation of the JM-resolving nuclease Mus81.

[*Keywords*: DNA damage response; cell cycle; post-replicative repair; homologous recombination; joint molecule resolution]

Supplemental material is available for this article.

Received February 24, 2014; revised version accepted June 4, 2014.

Intrinsically and extrinsically induced DNA lesions can compromise the integrity of the genetic information and threaten cell viability. DNA lesions are particularly dangerous during S phase, when faithful DNA replication relies on two intact DNA strands. DNA lesions hamper the progression of replication forks and thereby the complete duplication of chromosomes. Moreover, replication forks that are stalled at DNA lesion sites can collapse and cause chromosome breaks and genome instability (Branzei and Foiani 2010).

Eukaryotes possess two fundamentally different mechanisms to bypass DNA lesions that affect one of the parental DNA strands: translesion synthesis (TLS) and template switching. TLS employs specialized polymerases (translesion polymerases) that in many cases are able to replicate the damaged strand but with a reduced fidelity (Prakash et al. 2005). On the other hand, during template switching, the genetic information is copied from the newly synthesized, undamaged sister chromatid. This mechanism is therefore error-free in principle, yet its precise mechanism remains poorly understood. Template switching is a complex process that can be initiated by different recombination-based mechanisms (homologous recombination [HR] and error-free post-replicative repair [PRR]) (Branzei et al. 2008). The choice between the different bypass mechanisms is regulated by ubiquitin and SUMO modifications

[6]Present address: Max-Planck Institute of Biophysical Chemistry, Molecular Biology, 37077 Göttingen, Germany.
[7]These authors contributed equally to this work.
[8]Corresponding author
E-mail bpfander@biochem.mpg.de
Article is online at http://www.genesdev.org/cgi/doi/10.1101/gad.240515.114.

of the replication protein PCNA at sites of stalled replication forks (Pfander et al. 2005).

Template switch mechanisms involve the formation of DNA joint molecules (JMs; also referred to as sister chromatid junctions [SCJs] or X molecules) as repair intermediates (Branzei et al. 2008). In order to allow completion of DNA replication and faithful chromosome segregation, these X-shaped DNA structures need to be disentangled before sister chromatids are separated during mitosis. To date, three enzymatic activities—the topoisomerase-containing Sgs1–Top3–Rmi1 complex (STR) as well as the Mus81–Mms4 and Yen1 structure-specific endonucleases—were shown to process JMs in budding yeast (Liberi et al. 2005; Blanco et al. 2010; Mankouri et al. 2011; Szakal and Branzei 2013). These three activities can be distinguished by their mechanism (termed dissolution for STR and resolution for Mus81–Mms4 and Yen1) (Gaillard et al. 2003; Ip et al. 2008; Cejka et al. 2010) but show a partial functional overlap. Moreover, they are differentially regulated during the cell cycle: Whereas the STR activity appears to be cell cycle-independent, the activity of Mus81–Mms4 is stimulated by CDK-mediated and Cdc5 (budding yeast Polo-like kinase)-mediated phosphorylation and peaks in mitosis (Matos et al. 2011, 2013; Gallo-Fernández et al. 2012; Szakal and Branzei 2013). Accordingly, the Mus81 regulation is assumed to create a hierarchy, with STR acting as a primary resolution pathway and Mus81–Mms4 acting as a salvage pathway. How Mus81–Mms4 phosphorylation by cell cycle kinases facilitates this temporal regulation of JM resolution pathways remains hardly understood.

The bypass of DNA lesions during replication is additionally regulated by the DNA damage checkpoint, the main cellular signaling pathway in response to DNA damage (Harrison and Haber 2006). As the primary purpose of the checkpoint is the stabilization of stalled replication forks (Branzei and Foiani 2010), its activation is a fundamental requirement for all fork repair and reactivation reactions. Notably, the checkpoint has been suggested to be involved in the choice of the JM resolution pathway, since precocious activation of the Mus81–Mms4 endonuclease is observed in checkpoint-deficient mutants (Szakal and Branzei 2013). However, it remains to be clarified how this second layer of regulation of JM resolution is achieved on a molecular level and how it is linked to cell cycle regulation.

Here, we identify an evolutionarily conserved protein complex comprising two scaffold proteins, Slx4 and Dpb11/TopBP1, as an important regulator of JM resolution by Mus81–Mms4. We show that the formation of the Slx4–Dpb11 complex is regulated by the cell cycle stage. An *slx4* mutant, compromised specifically in Dpb11 binding, exhibits hypersensitivity to the replication fork-stalling drug MMS, a delay in the resolution of X-shaped DNA JMs, and a reduced propensity to form crossovers (COs). The function of the Slx4–Dpb11 scaffold in JM resolution correlates with the finding that Dpb11 binds to the Mus81–Mms4 endonuclease. This association is restricted to mitosis, since it is dependent on the mitotic kinase Cdc5. Moreover, the checkpoint acts antagonistically to the regulation of JM resolution by Slx4 and Dpb11, as we found that partial inactivation of the DNA damage checkpoint can compensate for defects in formation of the Slx4–Dpb11 scaffold complex.

Results

An evolutionarily conserved and phosphorylation-dependent interaction between Slx4 and Dpb11/TopBP1

Dpb11 and its human homolog, TopBP1, are critical regulators of the cellular DNA damage response and interact with several DNA replication, repair, and checkpoint proteins (Garcia et al. 2005; Germann et al. 2011). In these protein complexes, Dpb11/TopBP1 specifically binds to phosphorylated proteins via its tandem BRCT domains (Yu 2003; Garcia et al. 2005). A key role of Dpb11/TopBP1 is to function as a scaffold, bringing together specific sets of proteins via several interaction surfaces. In budding yeast, two Dpb11 complexes have been described in detail, which regulate replication initiation (with Sld3 and Sld2) (Tanaka et al. 2007; Zegerman and Diffley 2007) and the DNA damage checkpoint (with Rad9, the 9-1-1 complex, and Mec1–Ddc2) (Mordes et al. 2008; Navadgi-Patil and Burgers 2008; Puddu et al. 2008; Pfander and Diffley 2011), respectively (Fig. 1A). Recently, a third Dpb11 complex with Slx4 and Rtt107 was identified (Ohouo et al. 2010, 2012). In this latter complex, Slx4 appears to inhibit the formation of the Dpb11 DNA damage checkpoint complex (Ohouo et al. 2012).

In the course of our studies of Dpb11 function, we identified an interaction between a Dpb11 fragment that includes the tandem BRCT repeats 3 and 4 (BRCT3+4) and Slx4 using a two-hybrid screen. To confirm this finding, we tested the binding of different Dpb11 constructs to Slx4 and known Dpb11 binders. As observed before (Puddu et al. 2008; Pfander and Diffley 2011), we found that Rad9 binds to BRCT1+2 of Dpb11, whereas Ddc1 binds to BRCT3+4 (Fig. 1B). For Slx4, we found an interaction with full-length Dpb11 and the BRCT3+4 fragment but not with the BRCT1+2 domain (Fig. 1B). When we tested binding of Slx4 from cell extracts to recombinant, purified fragments of Dpb11, Slx4 also bound to BRCT3+4, albeit weaker than to the full-length protein (Supplemental Fig. S1A). Moreover, ablation of Dpb11 Thr451, which is predicted to be part of the BRCT3+4 phospho-protein-binding surface (Rappas et al. 2011), partially inhibited the Slx4–Dpb11 interaction (Supplemental Fig. S1B). A recent report suggested that the Dpb11 BRCT1+2 domain is involved in Slx4 binding (Ohouo et al. 2012). However, although our data do not rule out a contribution of BRCT1+2 in overall binding, our two independent lines of evidence clearly demonstrate that BRCT3+4 of Dpb11 significantly contributes to Slx4 binding.

Next, we mapped the Dpb11-binding site on Slx4 starting from a fragment (amino acids 461–738) that was common to all Slx4 clones identified in our initial Dpb11 two-hybrid screen. Truncated variants that begin at amino acid 490 failed to interact with Dpb11 (Supplemental Fig. S1C),

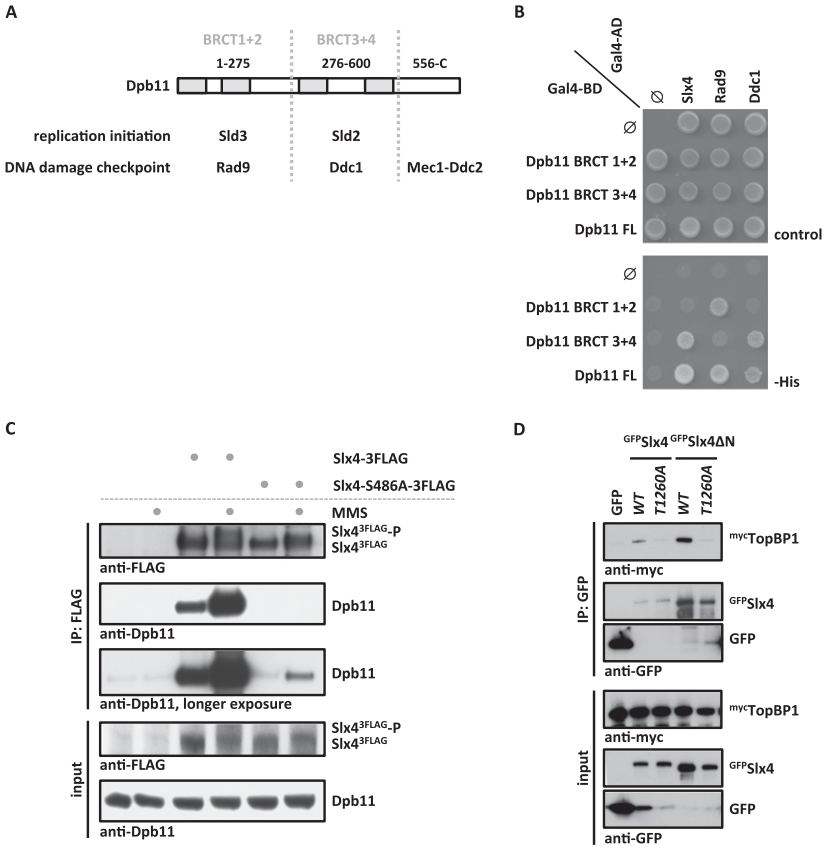

Figure 1. An evolutionarily conserved, phosphorylation-dependent interaction between Slx4 and Dpb11/TopBP1. (*A*) Schematic diagram of Dpb11 domain structure depicted with its interaction partners in replication initiation and DNA damage checkpoint. (*B*) Slx4 binds to the BRCT3+4 domain of Dpb11. Two-hybrid analysis of GAL4-BD fused to full-length Dpb11 or to BRCT1+2 and BRCT3+4 fragments and of GAL4-AD fusions with Slx4, Rad9, and Ddc1. (*C*) The Slx4–Dpb11 interaction is reduced by mutation of Slx4 Ser486 and is regulated by DNA damage. Coimmunoprecipitation of endogenous Dpb11 with Slx4^{3Flag} or phosphorylation-deficient Slx4-S486A^{3Flag} from undamaged cells or cells treated for 30 min with 0.033% MMS. (*D*) Human TopBP1 and Slx4 interact dependent on Thr1260 of Slx4. Coimmunoprecipitation of human ^{myc}TopBP1 with ^{GFP}Slx4 or N-terminally truncated ^{GFP}Slx4ΔN after transient overexpression in HEK293T cells. Slx4 or Slx4ΔN was expressed either as wild type (WT) or a T1260A phosphorylation-deficient variant.

indicating that the region between amino acid 461 and amino acid 490 is important for Dpb11 interaction. As several examples indicate that Dpb11 binds phosphorylated S/TP motifs, we tested all S/TP motifs within the C-terminal part of Slx4 for their ability to mediate Dpb11 binding. Indeed, we found that alteration of Ser486 in Slx4 into a nonphosphorylatable alanine residue (*slx4-S486A* mutant) reduced Dpb11 binding in a two-hybrid system (Supplemental Fig. S1D). Moreover, whereas immunoprecipitation of wild-type Slx4 efficiently copurified endogenous Dpb11 from cell extracts, in particular following MMS treatment, the Slx4–Dpb11 interaction was strongly decreased in extracts from cells expressing the *slx4-S486A* mutant, even after induction of DNA damage (Fig. 1C; see also Ohouo et al. 2012). Furthermore, the phospho-S486-containing peptide was specifically enriched (17-fold), when Dpb11 immunoprecipitations were analyzed by quantitative mass spectrometry (MS) (Supplemental Fig. S4A). We therefore conclude that the Slx4–Dpb11 interaction involves the BRCT3+4 region of Dpb11 and a region of Slx4 harboring the phosphorylated residue S486.

We further tested whether also the human homologs TopBP1 and Slx4 are binding partners. Indeed, we detected a specific interaction of TopBP1 and Slx4 or an N-terminally truncated version of Slx4 after transient transfection in human embryonic kidney (HEK) 293T cells (Fig. 1D). In contrast to the yeast proteins, we did not observe a stimulation of TopBP1 binding to Slx4 by DNA damage (Supplemental Fig. S1E). Human Slx4 is substantially larger than yeast Slx4, with an overall sequence conservation of only 17.9%. Nonetheless, we identified a conserved short linear motif present in Slx4 proteins from different eukaryotes that comprises Ser486 in budding yeast and Thr1260 in humans (Supplemental Fig. S2). Mutation of Thr1260 to a nonphosphorylatable alanine (T1260A) in human Slx4 reduced the interaction with TopBP1 (Fig. 1D), suggesting that this residue may function analogously to Ser486 in budding yeast. These data suggest the presence of a novel, evolutionarily conserved motif in Slx4 that functions in Dpb11/TopBP1 binding.

Cdk1-dependent phosphorylation of Slx4 regulates binding to Dpb11

In order to unravel the regulation of the Slx4–Dpb11-binding surface, we quantified the relative amount of Ser486 phosphorylation under different cellular conditions using SILAC-based quantitative MS. We observed a specific increase of Ser486 phosphorylation in G2/M-arrested cells compared with G1-arrested cells, indicating that the analyzed Slx4 phosphorylation is cell cycle-regulated (Fig. 2A). In agreement with Ser486 matching the consensus target sequence for phosphorylation by cyclin-dependent kinase Cdk1 (S/TPxK) (Holt et al. 2009), we observed a marked reduction of Ser486 phosphorylation in G2/M-arrested cells when Cdk1 activity was abrogated using the *cdc28-as1* allele (Bishop et al. 2000) in combination with 1NM-PP1 inhibitor treatment (Fig. 2B). Notably, we also detected

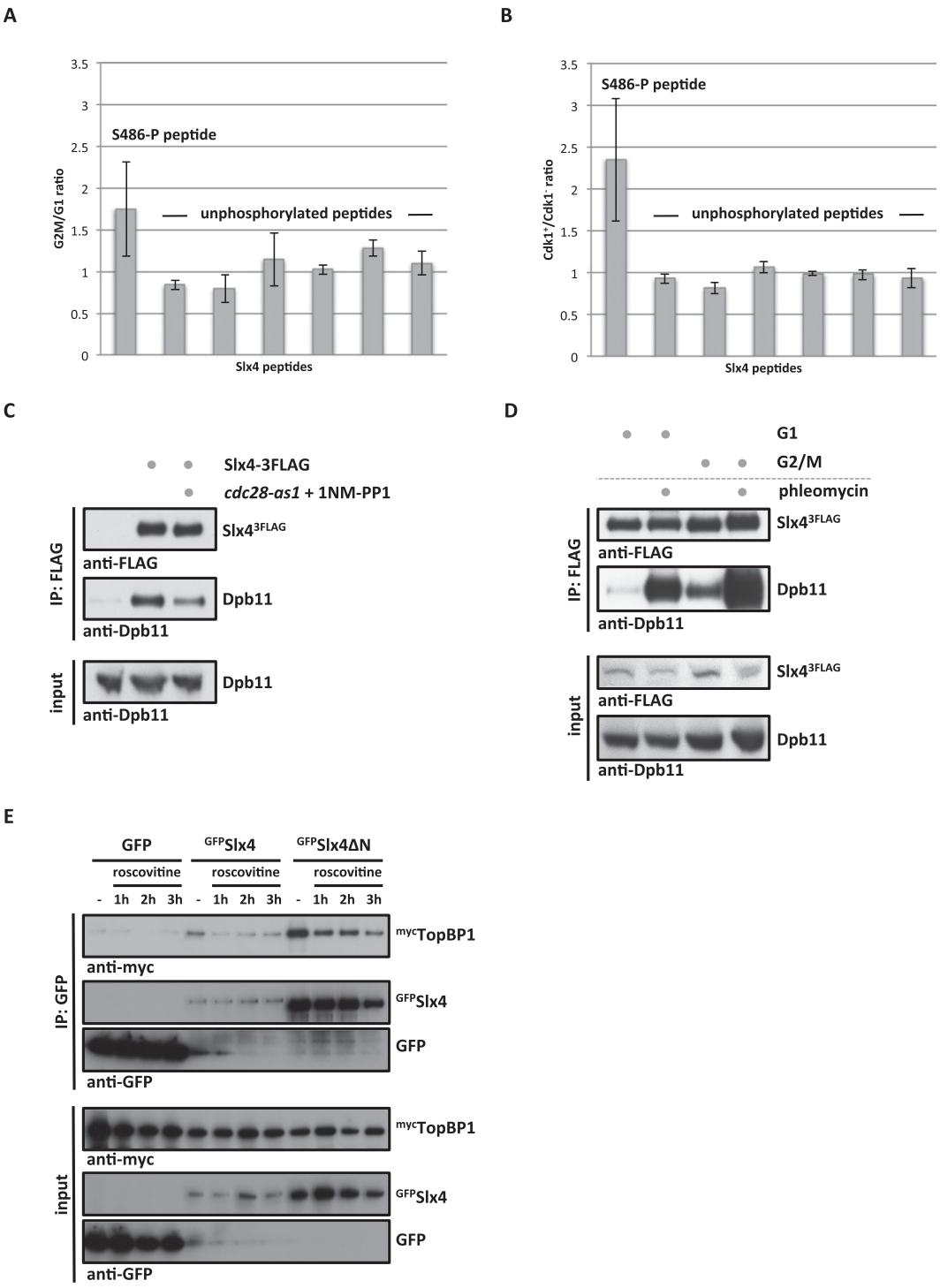

Figure 2. The Slx4–Dpb11/TopBP1-binding interface is cell cycle-regulated by Cdk1 phosphorylation of Slx4. (*A*) Ser486 phosphorylation is cell cycle-regulated. Relative abundance of the Slx4 480–489 phospho-peptide and six unmodified Slx4 peptides was measured by SILAC-based quantitative MS using $^{15}N_2{}^{13}C_6$ lysine (Lys8) and compared between Slx4 isolated from G1- and G2/M-arrested cells. H/L ratios for individual peptides were normalized to total Slx4 ratios. Error bars represent standard deviations from two independent experiments, including label switch. (*B*) S486 phosphorylation depends on Cdk1. Analysis as in *A* but comparing Slx4 from G2/M-arrested cells with normal Cdk1 activity with cells in which Cdk1 has been inactivated using the *cdc28-as1* allele and 500 nM 1NM-PP1. (*C*) The Slx4–Dpb11 interaction is regulated by CDK. Coimmunoprecipitation of Dpb11 and Slx4^{3Flag} from G2/M-arrested cells or G2/M-arrested cells in which Cdk1 has been inactivated as in *B*. (*D*) The Slx4–Dpb11 interaction is regulated by cell cycle phase and DNA damage. Experiment as in *C* but with G1- and G2/M-arrested cells, which were either damaged by 50 μg/mL phleomycin or left untreated. (*E*) Binding of human Slx4 and TopBP1 is regulated by CDK phosphorylation. Coimmunoprecipitation of ^{myc}TopBP1 with ^{GFP}Slx4 and ^{GFP}Slx4ΔN after transient overexpression in HEK293T cells. Cells were left untreated or treated with 10 μg/mL roscovitine for the indicated times to inhibit CDK activity.

reduced Slx4 binding to Dpb11 when Cdk1 was inhibited (Fig. 2C).

In addition to cell cycle-dependent regulation, we also observed a stimulation of Slx4–Dpb11 binding by DNA damage (Figs. 1C, 2D, Supplemental Fig. S1F). When Slx4 binding to recombinant GST-Dpb11 was tested, the DNA damage-dependent stimulation was less pronounced (Supplemental Fig. S1A), substantiating the notion that the Slx4–Dpb11 interaction may be additionally regulated by a damage-induced post-translational modification of Dpb11. On the other hand, Slx4 harbors several sites that can be targeted by kinases of the DNA damage checkpoint pathway. Mutation of seven sites in Slx4 partially inhibits its binding to Dpb11 (Ohouo et al. 2010), and the corresponding mutant shows phenotypes similar to those of *slx4-S486A* (Supplemental Fig. S3). As we cannot fully exclude pleiotropic defects for this mutant, we focused our analysis on *slx4-S486A*.

Taken together, our findings suggest that the Slx4–Dpb11 complex integrates at least two cellular signals: (1) cell cycle state through Cdk1 phosphorylation of Slx4 at Ser486 and (2) the presence of DNA damage through checkpoint kinase phosphorylation of several sites on Slx4 and perhaps on Dpb11.

Interestingly, the CDK regulation of this interaction is conserved between yeast and humans, since addition of the CDK inhibitor roscovitine reduced binding of Slx4 and TopBP1 (Fig. 2E).

The Slx4–Dpb11 complex is required for the response to replication fork stalling

Budding yeast Slx4 is known to bind to several DNA repair proteins (Slx1, Rtt107, and Rad1–Rad10) (Mullen et al. 2001; Roberts et al. 2006; Flott et al. 2007; Ohouo et al. 2010). However, whether these interaction partners are part of only one or several distinct complexes is unknown. While Slx4 has several independent DNA repair functions in budding yeast (Flott et al. 2007), until now, a detailed phenotypic characterization has only been conducted for *slx4Δ* deletion mutants. To test the specificity of the Dpb11-binding-deficient *slx4-S486A* phosphorylation site mutant, we compared its binding partners with those of wild-type Slx4 using quantitative proteomics. Indeed, we found that the mutant protein (Slx4-S486A^{3Flag}) displayed eightfold reduced binding to Dpb11 (Fig. 3A). This variant still bound Slx1 and Rtt107 as efficiently as wild-type Slx4, indicating that Ser486 phosphorylation is specifically relevant for the Dpb11 interaction (Fig. 3A; see Supplemental Fig. S4A for specific Slx4 interactors). We thus took advantage of the *slx4-S486A* separation-of-function mutant to reveal a specific role of the Slx4–Dpb11 complex.

Using different DNA-damaging agents, we observed that the *slx4-S486A* mutant is particularly sensitive to MMS and, to a lesser extent, 4-NQO (Fig. 3B; Supplemental Fig. S4B), two reagents that create toxicity through replication fork stalling. Notably, the mutant was not sensitive to reagents that generate DNA strand breaks or interstrand cross-links, consistent with a recombination rate that was similar to wild type (Supplemental Fig. S4B,C). Remarkably, expression of a fusion protein of the phospho-site mutant variant of Slx4 with Dpb11 (Dpb11–Slx4-S486A) rescued the MMS hypersensitivity phenotype almost to wild-type levels (Fig. 3B), suggesting that binding of Slx4 to Dpb11 is crucial for tolerance of replication fork-stalling lesions.

Next, we tested whether the response to stalled replication forks is aberrant in the *slx4-S486A* mutant. To this end, we treated synchronized cells with a pulse of MMS in early S phase. Under these conditions, the *slx4-S486A* mutant completed DNA replication with slightly slower kinetics compared with wild-type cells (Fig. 3C, 1-h time point). Also, the appearance of fully replicated and repaired chromosomes, as visualized by pulsed-field gel electrophoresis, was delayed (Fig. 3D, 1-h time point). This finding indicates that stalled replication fork structures or repair intermediates persist longer in the absence of the Slx4–Dpb11 complex. Additionally, the DNA damage checkpoint activation was prolonged in *slx4-S486A* cells (Fig. 3E), as determined by the phosphorylation status of the checkpoint kinase Rad53. This effect was specific for MMS treatment and could not be observed in cells in which double-strand breaks were induced by zeocin or phleomycin inside or outside of S phase (Supplemental Fig. S4D).

Defects in a checkpoint-antagonistic pathway (checkpoint "dampening") (Ohouo et al. 2012) in *slx4* mutants could, in principle, lead to prolonged checkpoint activation and could thereby indirectly lead to slow S-phase kinetics and DNA damage hypersensitivity. Alternatively, persistence of unrepaired DNA lesions or DNA repair intermediates could lead to very similar phenotypes. In order to discriminate between the two possibilities, we examined the DNA damage levels during recovery from an MMS pulse in wild-type and *slx4-S486A* cells. To this end, we investigated the appearance and disappearance of nuclear foci formed by the ssDNA-binding protein RPA after MMS treatment in S phase. Indeed, *slx4-S486A* cells contained more RPA foci, which persisted longer than in wild-type cells (Fig. 3F). Therefore, we conclude that unrepaired DNA lesions or DNA repair intermediates that contain ssDNA persist in *slx4-S486A* mutants. This finding does not necessarily exclude a role of Slx4 as a regulator of the DNA damage checkpoint yet strongly suggests an additional direct function of the Slx4–Dpb11 complex in the repair of replication fork structures.

The Slx4–Dpb11 complex promotes Mus81–Mms4-dependent JM resolution

As our findings pointed to a function of the Slx4–Dpb11 complex in the response and repair of MMS-induced lesions, we next investigated whether the complex is involved in the DNA damage bypass. Therefore, we tested possible functions in HR and error-prone or error-free PRR. From several lines of genetic evidence, we conclude that the Slx4–Dpb11 complex is not exclusively involved in either PRR or HR (Supplemental Fig. S5). First, the *slx4-S486A* mutation enhanced the MMS hypersensitivity of mutants defective in error-free PRR (double mutant with either *mms2Δ*, *rad5-KT538,539AA*,

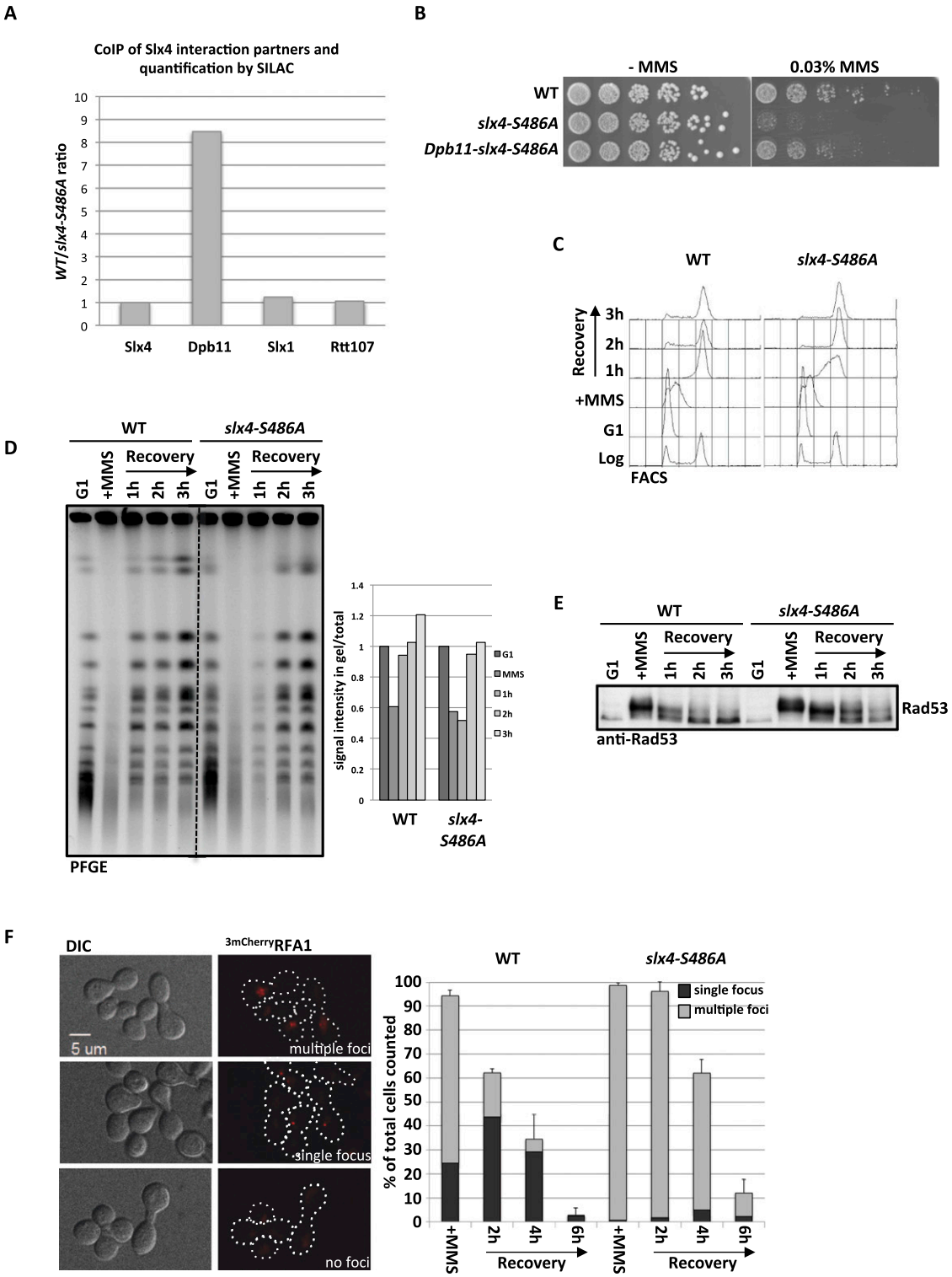

Figure 3. Mutation of *slx4-S486A* results in a specific defect in binding to Dpb11 and the response to stalled replication forks. (*A*) The *slx4-S486A* mutant leads to a specific defect in binding to Dpb11. Relative enrichment of Slx4 interactors (see Supplemental Fig. S4A) found in purifications of wild-type (WT) $Slx4^{3Flag}$ versus $Slx4\text{-}S486A^{3Flag}$ as determined by SILAC-based quantitative MS. Values >1 indicate a reduced binding to the Slx4-S486A relative to wild-type Slx4. (*B*) The *slx4-S486A* mutant, but not a *Dpb11–slx4-S486A*-fusion, is hypersensitive to MMS. Wild type or strains expressing *slx4-S486A* or the *Dpb11–slx4-S486A*-fusion from the *SLX4* promoter as only a copy of *SLX4* were spotted in fivefold serial dilutions on MMS-containing medium and assayed for growth after 2 d. (*C*,*D*) Replication fork stalling is prolonged in the *slx4-S486A* mutant. Cells were treated with a pulse of MMS during S phase, and recovery was analyzed by FACS (*C*; to measure cellular DNA content) and pulsed-field gel electrophoresis (*D*; to measure intact, fully replicated chromosomes). (*D*) For quantification, the fluorescence signal of chromosomes that migrated into the gel was divided by the total signal, including the pocket, and all signals were normalized to the G1 sample from each strain. (*E*) The DNA damage checkpoint is inactivated with reduced kinetics in the *slx4-S486A* mutant. Cells were treated as in *C*, and checkpoint activity was determined by anti-Rad53 Western blot. (*F*) The *slx4-S486A* mutant shows increased DNA damage foci and delayed recovery after transient MMS treatment in S phase. DNA damage sites were visualized by the ssDNA-binding $RFA1^{3mCherry}$ after transient MMS treatment during S phase. Cells were sorted into three categories: multiple, dispersed RFA1 foci; one RFA1 focus; and no RFA1 foci. Values are from two independent experiments, counting 100–150 cells per strain and time point. Error bars represent standard deviations.

or *rad5-C914S*), error-prone PRR (double mutant with either *rev1Δ*, *rev3Δ*, or *rad30Δ*), or HR (double mutant with *rad51Δ*) (Supplemental Fig. S5A). Second, spontaneous mutagenesis, a hallmark of error-prone PRR, was not significantly altered in *slx4-S486A* mutants (Supplemental Fig. S5B). Third, recombination rates, as determined by a direct repeat recombination assay, were similar between wild-type and *slx4-S486A* strains (Supplemental Fig. S4C). Fourth, *siz1Δ* or *srs2ΔC* mutations, which cause an upregulation of HR at stalled replication forks (Pfander et al. 2005), did not alleviate the MMS hypersensitivity of *slx4-S486A* mutants (Supplemental Fig. S5C).

The nonepistatic relationship of the *slx4-S486A* mutant to PRR or HR pathways could be explained if Slx4 and Dpb11 participated in a step common to both error-free PRR and HR because, in such a scenario, both pathways would be affected by the *slx4-S486A* mutation. Both HR and error-free PRR operate via template switching in order to bypass the replication fork-stalling lesion by copying the undamaged information from the sister chromatid. A critical step in template switching is the final removal of X-shaped DNA intermediates (JMs) that link the two sister chromatids (Mankouri et al. 2013). JM removal pathways act, in principle, independently of the pathway by which JMs have been created (Branzei et al. 2008; for *mus81Δ* phenotypes, see Interthal and Heyer 2000; Li and Brill 2005). To test whether the Slx4–Dpb11 complex is involved in this late step, we visualized these DNA intermediates in an *sgs1Δ* mutant (deficient in JM dissolution) by two-dimensional (2D) gel electrophoresis (Liberi et al. 2005; Mankouri et al. 2011). In this mutant, MMS treatment in S phase leads to enhanced levels of JMs, which subsequently disappear during late S, G2, and M phase (Szakal and Branzei 2013). The additional mutation of *slx4-S486A* in the *sgs1Δ* background does not alter the formation of JMs, indicating that the Slx4–Dpb11 complex is not required at early steps (Supplemental Fig. S6A). Interestingly, however, during the recovery from the MMS treatment, JMs are more slowly resolved in the *sgs1Δ slx4-S486A* double mutant compared with the *sgs1Δ* single mutant (Fig. 4A). A similar effect can be observed using an *slx4Δ* mutant and conditionally inactivated *SGS1* in the same experimental setup (Supplemental Fig. S6B). Consistently, we observed an enhanced MMS sensitivity for the *sgs1Δ slx4-S486A* double mutant compared with the respective single mutants (Fig. 4B). From these experiments, we conclude that the Slx4–Dpb11 complex is involved in the resolution of JMs that are supposedly intermediates arising from a template switch reaction and that this complex functions in a pathway parallel to dissolution by the STR complex.

To elucidate a potential role of the Slx4–Dpb11 complex in a resolution mechanism, we investigated the genetic interaction with Mus81–Mms4. Indeed, the MMS sensitivities of *slx4-S486A mms4Δ* or *slx4-S486A mus81Δ* double mutants were identical to those of *mms4Δ* or *mus81Δ* single mutants (Fig. 4C). This suggests that the Slx4–Dpb11 complex acts in the Mus81–Mms4 pathway. The same epistatic relationship was seen between *mms4Δ* and *slx4-S486A* when we investigated JM resolution by 2D gel electrophoresis when the STR complex was inactivated using the *Tc-sgs1* allele (Supplemental Fig. S6C). We note that the MMS hypersensitivity and the JM resolution defect of the *slx4-S486A* mutant are less pronounced compared with the deletion mutants that fully abolish Mus81 function (Fig. 4C; Supplemental Fig. S6C), suggesting that not all functions of the Mus81–Mms4 endonuclease depend on the Slx4–Dpb11 complex.

We also tested the involvement of other structure-specific endonucleases (Slx1, Rad1–Rad10, and Yen1) (Tomkinson et al. 1993; Fricke and Brill 2003; Coulon 2006; Ip et al. 2008), specifically of Slx1, as it associates with the Slx4–Dpb11 complex (Supplemental Fig. S4A). We found that *rad1Δ* showed an additive phenotype with *slx4-S486A*, while *slx1Δ* and *yen1Δ* mutants were not hypersensitive to MMS (Supplemental Fig. S6D; Fricke and Brill 2003; Coulon 2006; Blanco et al. 2010). We therefore conclude that these factors either are not involved in the resolution of template switch intermediates by Mus81 and the Slx4–Dpb11 complex or (in case of Slx1 and Yen1) have a function that can be taken over by a redundant pathway in the respective deletion mutant. Interestingly, the *yen1Δ* mutation caused an increase of MMS sensitivity specifically of the *sgs1Δ slx4-S486A* double mutant (Supplemental Fig. S6E), suggesting that Yen1 function becomes specifically important if the STR complex is inactive and function of the Slx4–Dpb11 complex is reduced.

The balance between STR-dependent JM dissolution and Mus81-dependent JM resolution is reflected in the ratio of CO to non-CO (NCO) products (Ira et al. 2003; Ho et al. 2010; Mankouri et al. 2013), since STR-mediated dissolution will not yield COs, while Mus81-mediated resolution can generate CO products. We therefore analyzed the rates of CO formation in the *slx4-S486A* mutant with a recombination assay using interchromosomal *arg4* heteroalleles (Robert et al. 2006; Szakal and Branzei 2013). Despite a slight increase in overall recombination rates, we measured a reduction in CO rates in the *slx4-S486A* mutant compared with wild-type cells (Fig. 4D). We therefore conclude that the Slx4–Dpb11 complex is an important regulator of JM removal pathways and that it acts by stimulating JM resolution, inhibiting JM dissolution, or both.

Persistent JMs interfere with the separation of sister chromatids in mitosis. Under circumstances in which JMs are not resolved before anaphase, these repair intermediates are thought to give rise to anaphase bridges between the dividing DNA masses (Chan et al. 2007; Mankouri et al. 2013). Consistent with a role in the resolution of JMs, Dpb11 localizes to DNA bridges between the separated chromosome masses in anaphase (Germann et al. 2014). Dpb11-containing anaphase bridges can be observed with a low frequency in undamaged cells (<5%) and are induced upon MMS treatment, suggesting that they arise from replication fork stalling (Germann et al. 2014). Interestingly, the occurrence of Dpb11 bridges is increased in *sgs1Δ* cells (Germann et al. 2014), indicating that the localization of Dpb11 to chromatin bridges reflects its action in a resolution mechanism. We observed a pro-

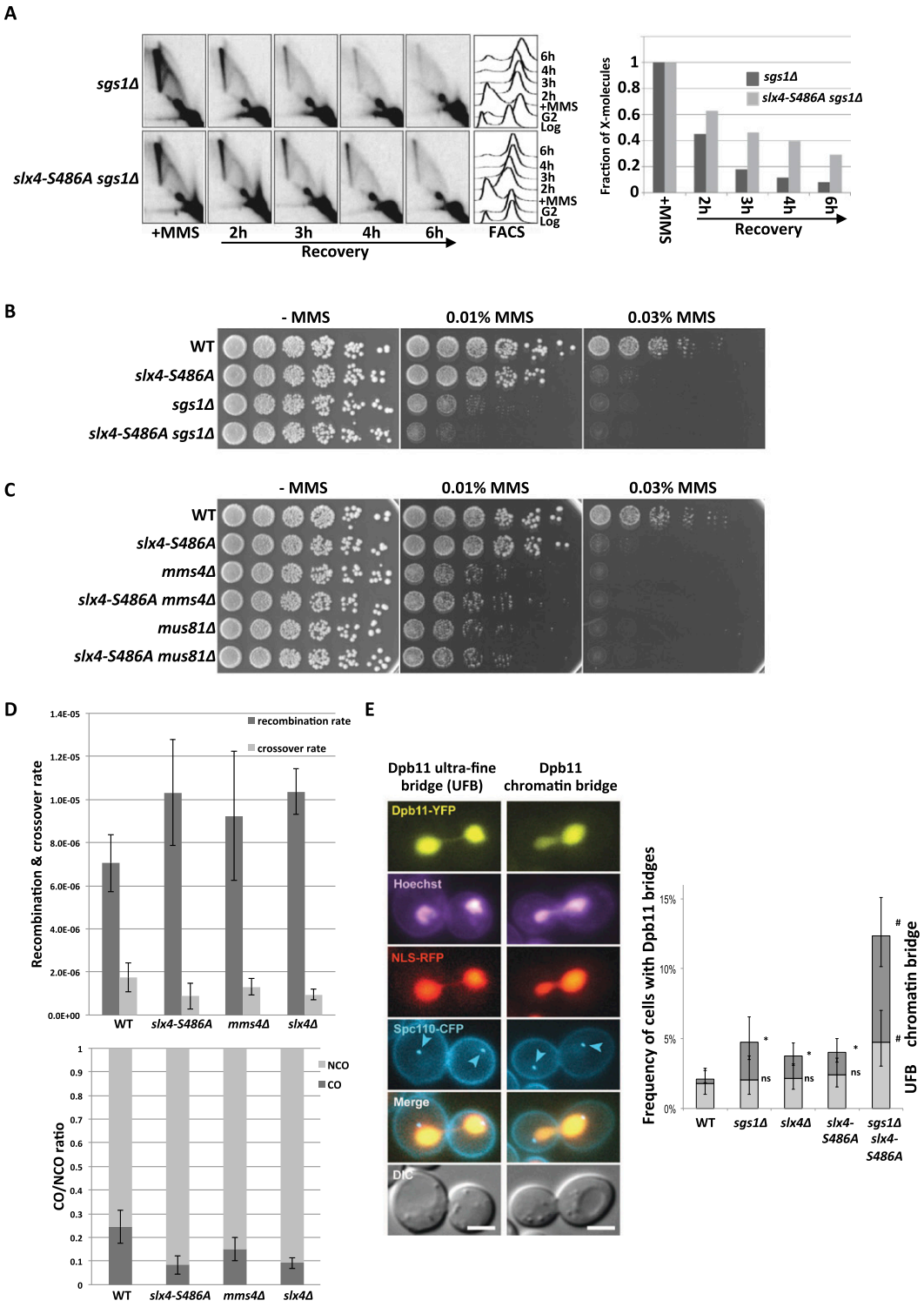

Figure 4. The Dpb11 binding-deficient *slx4-S486A* mutant causes defects in the Mus81–Mms4-dependent JM resolution. (*A*) JM structures are resolved slower in *sgs1Δ slx4-S486A* cells. X-shaped JMs were visualized as spike signal in 2D gels in *sgs1Δ* and *sgs1Δ slx4-S486A* cells that have been treated with a pulse of MMS in S phase. (*B*) MMS sensitivity is enhanced in the *sgs1Δ slx4-S486A* double mutant compared with each single mutant. Analysis of the MMS hypersensitivity phenotype as in Figure 3B. (*C*) The MMS hypersensitivity of *mms4Δ* and *mus81Δ* mutants is not further enhanced by an additional *slx4-S486A* mutation. Experiment as in *B*. (*D*) The *slx4-S486A* mutation leads to a reduced CO formation. COs and NCOs from an interchromosomal recombination assay using *arg4* heteroalleles on chromosome V and VIII (Robert et al. 2006) were determined using a PCR-based strategy. (*Top* panel) Recombination and CO rates were determined by fluctuation analysis using a maximum likelihood approach. (*Bottom* panel) CO ratio is quotient of CO rate and overall recombination rate. Error bars represent standard deviations of two to 11 independent experiments. (*E*) Dpb11 anaphase bridge structures occur more frequently when JM dissolution and the Dpb11–Slx4 interaction are defective. (*Right* panel) Quantification of Dpb11 ultrafine bridges (UFBs) or chromatin bridges in wild-type (WT), *sgs1Δ*, *slx4Δ*, *slx4-S486A*, and *slx4-S486A sgs1Δ* strains. Cells express Dpb11-YFP, NLS-RFP as a marker of the nucleoplasm and Spc110-CFP as a marker of the spindle pole body. DNA is stained with Hoechst. (*Left* panel) Images of representative anaphase cells are shown. Bar, 3 μm. Error bars indicate 95% confidence intervals. Significance is as follows: (*) $P < 0.01$ (compared with wild type); (#) $P < 0.01$ (compared with the single mutants); (ns) not significantly different from wild type.

nounced increase of cells containing Dpb11 bridges when the *sgs1Δ* and *slx4-S486A* mutants were combined (Fig. 4E). The genetic requirements for Dpb11 bridges are therefore highly similar to those for persistent JMs (Fig. 4A), supporting a role for Dpb11 and Slx4 in JM resolution. In line with this model, we observed frequent colocalization of either $Slx4^{YFP}$ or $Mus81^{YFP}$ with $Dpb11^{CFP}$-positive bridges that is further enhanced in *sgs1Δ* cells (Supplemental Fig. S7A). We also noticed a colocalization of Slx4, Mus81, and Dpb11 in DNA damage foci yet to a lesser extent (Supplemental Fig. S7B). Overall, the data in Figure 4 provide strong support for an involvement of the Slx4–Dpb11 complex in JM resolution by Mus81–Mms4.

Mus81–Mms4 interacts with the Slx4–Dpb11 complex during mitosis in a Cdc5-dependent fashion

To elucidate how the Slx4–Dpb11 complex regulates Mus81 function, we investigated a possible physical interaction. In previous studies using asynchronously growing yeast cells, no binding of Slx4 to Mus81–Mms4 was detectable (Schwartz et al. 2012). However, we detected Mms4 as a cell cycle-specific interactor if $Slx4^{3Flag}$ immunoprecipitations were investigated by SILAC MS (such as in Fig. 2A). Moreover, when we arrested cells in G2/M by nocodazole treatment, immunopurification of $Mms4^{3Flag}$ copurified Dpb11 and Slx4 (Fig. 5A). Notably, this interaction is highly cell cycle-specific, as it could not be observed in G1- or S-phase cells (Fig. 5A). We determined, using an unbiased SILAC MS approach, that Dpb11, Slx4, and Rtt107 are among the best interactors of Mus81–Mms4 in G2/M-arrested cells (Supplemental Fig. S8A).

Next, we tested whether Dpb11, Slx4, and Mus81–Mms4 form a single protein complex. Indeed, the three proteins comigrated at a size of ~33 S (Supplemental Fig. S8B, fractions 18–20, apparent molecular weight 1.1–1.2 MDa) when the eluate of an $Mms4^{3Flag}$ purification from G2/M cells was subjected to a glycerol gradient centrifugation. When we analyzed the complex architecture by a two-hybrid approach, we detected a direct interaction of Dpb11 and Mms4 that is independent of Slx4 (Supplemental Fig. S8C). Moreover, when we immunoprecipitated $Mms4^{3Flag}$ in the *slx4-S486A* background, we observed a reduction of Slx4, but not Dpb11, binding to $Mms4^{3Flag}$ (Fig. 5B). These findings thus suggest that Dpb11, Slx4, and Mus81–Mms4 are part of a multiprotein complex in which Dpb11 acts as a bridge between Slx4 and Mus81–Mms4.

We observed that Dpb11 and Slx4 could be partially eluted from Mms4-containing beads using λ-phosphatase treatment (Supplemental Fig. S8D), suggesting that the binding is at least in part dependent on protein phosphorylation. Previous work has established that Mus81 activity is decisively up-regulated in mitosis in response to a sequential phosphorylation of Mms4 by CDK and the Polo-like kinase Cdc5 (Matos et al. 2011; Gallo-Fernández et al. 2012; Saugar et al. 2013; Szakal and Branzei 2013). We therefore used two systems to interfere with Cdc5 activity: the *cdc5-as1* analog-sensitive allele, which we inhibited using chloromethylketone (CMK) (Snead et al. 2007), and transcriptional shutoff of *pGAL-CDC5* using glucose repression. Both types of Cdc5 inactivation resulted in a loss of the slower-migrating species of Mms4 in gels and at the same time diminished the binding of Dpb11 and Slx4 to $Mms4^{3Flag}$ (Fig. 5C; Supplemental Fig. S9A). In order to rule out indirect effects, we tested whether Cdk1 activity was uninfluenced under conditions of Cdc5 inhibition/shutoff and saw that neither the interaction between Slx4 and Dpb11 nor phosphorylation of a CDK target site on Rad9 (T474) (Pfander and Diffley 2011) was influenced by Cdc5 inactivation (Supplemental Fig. S9B,C). Together with our results on the architecture of the Slx4–Dpb11–Mms4–Mus81 complex, these experiments suggest that binding of Mms4 to Dpb11 is regulated by Cdc5 phosphorylation.

We also tested whether the formation of the Slx4–Dpb11–Mms4–Mus81 was regulated upon DNA damage. We found that $Mms4^{3Flag}$ bound similar amounts of Dpb11 and Slx4 after phleomycin or mock treatment of G2/M-arrested cells (Supplemental Fig. S9D). Moreover, we could also observe formation of the Slx4–Dpb11–Mms4–Mus81 complex during recovery from MMS pulse treatment during S phase (Fig. 5D). However, this binding occurred only once Cdc5 became active, as visualized by the slower-migrating form of Mms4, indicating that even after DNA damage, the Dpb11–Mms4 interaction is dependent on Cdc5 (Fig. 5D).

Given that the cell cycle regulation of Mus81 activity and the cell cycle regulation of the Slx4–Dpb11–Mms4–Mus81 complex formation have the same requirements, we tested whether the up-regulation of Mus81 nuclease activity requires Slx4 and Dpb11. We analyzed in vitro resolution of nicked Holliday junctions, Holliday junctions, and model replication fork structures on immunopurified Mus81–Mms4 and found that the enhanced activity of mitotic Mus81 is similar, independently of whether Mus81 was purified from wild-type or *slx4-S486A* cells (Fig. 5E; Supplemental Fig. S9E). Therefore, we conclude that cell cycle kinases regulate Mus81 by at least two mechanisms: direct up-regulation of the catalytic activity, which can be reconstituted in vitro, and an up-regulation through formation of an Slx4–Dpb11–Mms4–Mus81 complex, which could be seen in vivo.

The DNA damage checkpoint regulates the Slx4–Dpb11-dependent Mus81 function

The DNA damage checkpoint prevents collapse of stalled replication forks and thereby is fundamentally required for all aspects of the response to stalled replication forks (Branzei and Foiani 2010). Moreover, the checkpoint was also suggested to counteract Cdc5-dependent Mus81 activation, since premature Mms4 phosphorylation by Cdc5 was observed after MMS treatment of checkpoint-deficient cells (Szakal and Branzei 2013). Possible explanations for this phenomenon are a faster S-phase progression in the checkpoint mutants or a direct inhibition of Cdc5 activity by the checkpoint (Zhang et al. 2009).

To address these possibilities, we investigated the influence of the DNA damage checkpoint on Slx4–Dpb11–Mms4–Mus81 complex function. Interestingly, we found

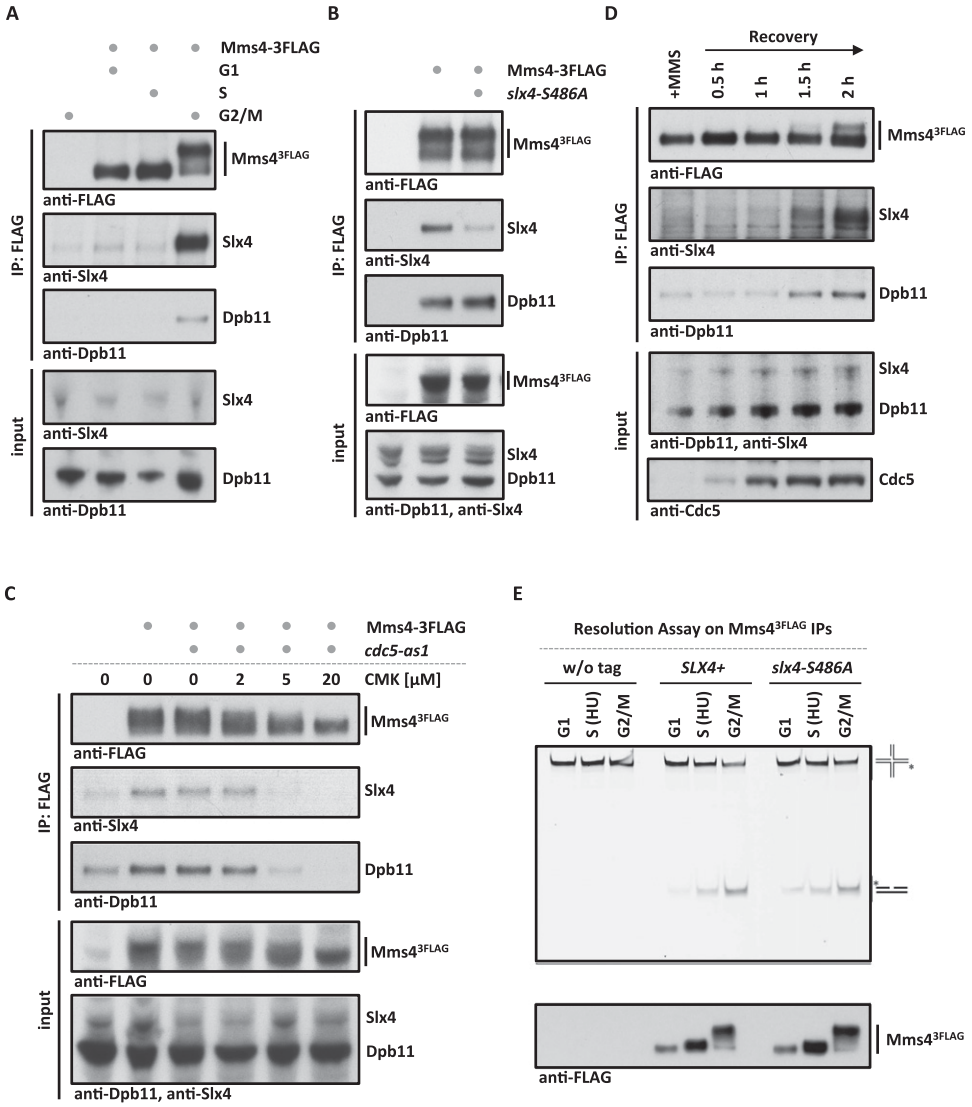

Figure 5. Slx4, Dpb11, and Mus81–Mms4 form a Cdc5-dependent complex at the G2/M cell cycle stage. (*A*) Mms4 binds to Dpb11 and Slx4 specifically in G2/M. Coimmunoprecipitation samples of Mms4^{3Flag} from G1, S, or G2/M cells were tested for binding to Dpb11 and Slx4. (*B*) Slx4-S486A is partially lost from the Slx4–Dpb11–Mms4–Mus81 complex, suggesting that Dpb11 bridges the interaction between Mms4 and Slx4. Mms4^{3Flag} coimmunoprecipitation were carried out as in *A* but from G2/M-arrested wild-type (WT) or *slx4-S486A* mutant cells. (*C*) The Dpb11–Mms4 interaction is dependent on the Polo-like kinase Cdc5. *cdc5-as1* was inhibited by 2, 5, and 20 μM CMK in G2/M-arrested cells. Mms4^{3Flag} coimmunoprecipitation was performed as in *A*. (*D*) Cdc5 hyperphosphorylated Mus81–Mms4 binds to Slx4 and Dpb11 during recovery from MMS damage. Cells were treated with a 30-min pulse of 0.03% MMS. Mms4^{3Flag} coimmunoprecipitations were performed from samples after 0, 30, 60, 90, and 120 min of recovery in nocodazole-containing medium. (*E*) Cell cycle regulation of Mus81–Mms4 nuclease activity remains intact in the *slx4-S486A* mutant. Mms4^{3Flag} and control immunoprecipitations (see the *bottom* panel for immunoprecipitation samples) from cells arrested in their cell cycle by α factor, HU, or nocodazole were incubated with a fluorescence-labeled nicked Holliday junction substrate.

that a partial defect in DNA damage checkpoint signaling alleviated the phenotypes of the *slx4-S486A* mutant (Fig. 6A,B; Supplemental Fig. S10A,B; see also Ohouo et al. 2012). In these experiments, we used three distinct mutants, which were partially impaired in checkpoint signaling: *ddc1-T602A* (defective in Dpb11-dependent Rad9 recruitment (Puddu et al. 2008), *dot1Δ* (defective in chromatin-dependent Rad9 recruitment) (Giannattasio et al. 2005), and *rad53-3HA* (a hypomorphic Rad53 allele) (Cordon-Preciado et al. 2006). All three mutants partially suppressed the hypersensitivity of *slx4-S486A* to chronic exposure of MMS (Fig. 6A; Supplemental Fig. S10A). Furthermore, the recovery from MMS treatment as judged by the reappearance of fully replicated chromosomes in PFGE and reappearance of unphosphorylated Rad53 was enhanced in *slx4-S486A ddc1-T602A* cells compared with *slx4-S486A* cells (Fig. 6B; Supplemental Fig. S10B).

A plausible interpretation of these results is that a partial inactivation of the checkpoint may compensate for a reduced or delayed formation of the Slx4–Dpb11–Mms4–

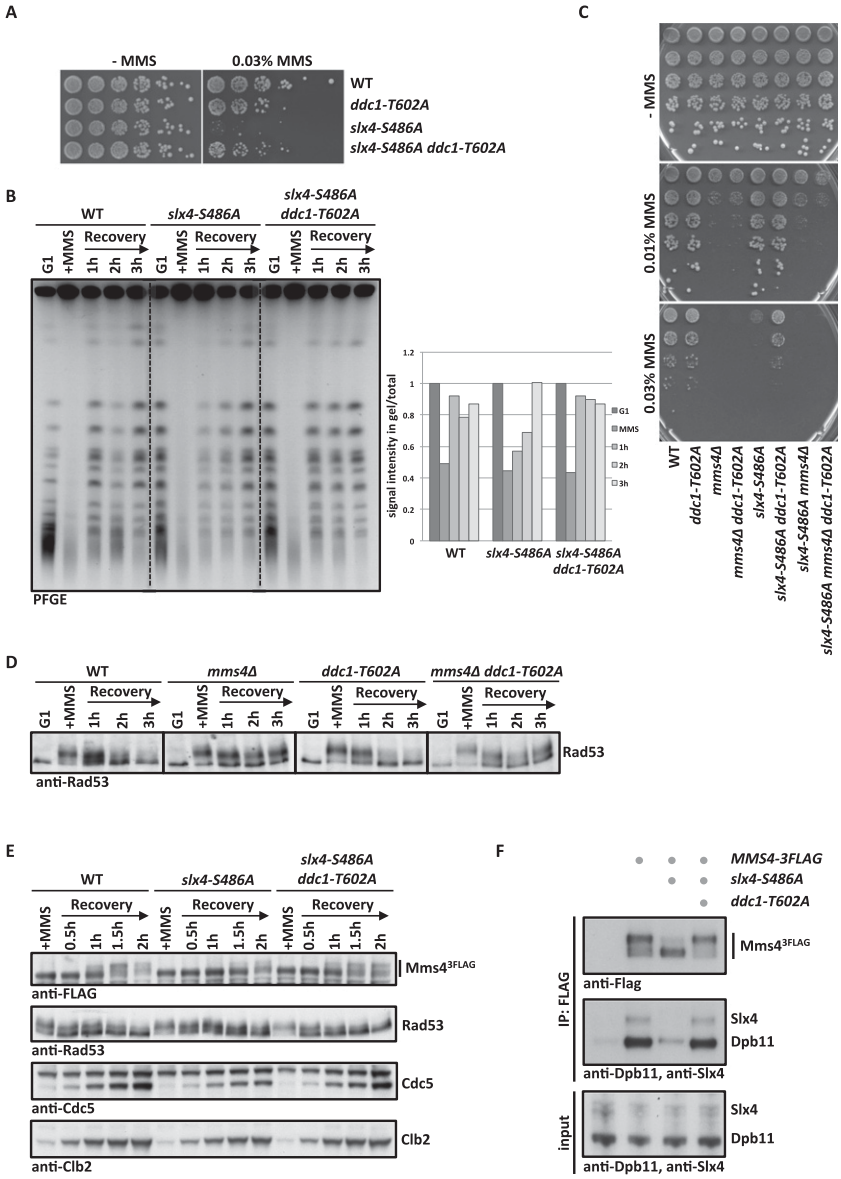

Figure 6. Partial inactivation of the DNA damage checkpoint rescues *slx4-S486A* phenotypes in an *MMS4*-dependent manner. (*A*) The DNA damage repsonse defect of *slx4-S486A* is suppressed by partial inactivation of the DNA damage checkpoint. Wild type (WT), *slx4-S486A*, the partial checkpoint mutant *ddc1-T602A*, and the *slx4-S486A ddc1-T602A* double mutant were spotted in fivefold serial dilutions on MMS-containing plates. (*B*) The prolonged replication fork stalling of the *slx4-S486A* mutant is rescued by the *ddc1-T602A* mutation. Cells were cell cycle-synchronized and treated with a 30-min pulse of 0.033% MMS in S phase. Recovery of fully replicated chromosomes was analyzed by pulsed-field gel electrophoresis. Quantification as in Figure 3D. (*C*) A complete defect in Mus81 activity (*mms4Δ*) cannot be rescued by checkpoint inactivation. The MMS hypersensitivity phenotypes of *slx4-S486A*, *mms4Δ*, and *ddc1-T602A* mutants and double and triple mutant combinations were analyzed as in *A*. (*D*) The checkpoint recovery defect of *mms4Δ* mutants is not rescued by a partial checkpoint mutant. Cells were treated as in *B*, and checkpoint activity was measured by Rad53 phosphorylation. (*E*,*F*) Cdc5-dependent hyperphosphorylation of Mms4 and concomitant binding to Dpb11 and Slx4 occur earlier during recovery from replication fork stalling in *slx4-S486A ddc1-T602A* double mutants compared with *slx4-S486A* mutants. (*E*) Cells were treated with a 40-min pulse of 0.033% MMS in S phase. The Cdc5-dependent $Mms4^{3Flag}$ phosphorylation shift was measured by anti-Flag Western blot, checkpoint activity was measured by Rad53 phosphorylation, and cell cycle progression was followed by anti-Clb2 and anti-Cdc5 Westerns. (*F*) Wild-type, *slx4-S486A*, and *slx4-S486A ddc1-T602A* cells that contain $MMS4^{3Flag}$ were harvested during the recovery phase (2.5 h after MMS removal) and subjected to anti-Flag immunoprecipitation. Coimmunoprecipitation samples were tested for binding to Dpb11 and Slx4.

Mus81 complex. Such compensation may occur by either a direct up-regulation of the Slx4–Dpb11–Mms4–Mus81 complex or hyperactivation of a Mus81-independent salvage pathway. We therefore tested whether the observed rescue would depend on Mms4. Consistent with a direct influence of the checkpoint on the Slx4–Dpb11–Mms4–Mus81 complex, a partial inactivation of the checkpoint did not rescue the MMS hypersensitivity of the *mms4Δ* or *mms4Δ slx4-S486A* mutants (Fig. 6C). In contrast, the *sgs1Δ slx4-S486A* or *yen1Δ slx4-S486A* double mutants could be rescued by additional mutation of *ddc1-T602A* (Supplemental Fig. S10C), suggesting that neither STR nor Yen1 activity is required for the rescue. Furthermore, *mms4Δ ddc1-T602A* mutants show a slow checkpoint recovery after a pulse of MMS in S phase that is similar to *mms4Δ* cells (Fig. 6D). These results suggest that the rescue of *slx4-S486A* mutants upon partial checkpoint inactivation is due to the action of Mms4–Mus81.

Furthermore, when we transiently exposed cells to MMS during S phase and released them into a G2/M arrest, we observed that the Cdc5-dependent phosphorylation shift of Mms4, which in this experiment serves as a marker for the interaction with Slx4–Dpb11, was slightly delayed in *slx4-S486A* cells compared with wild-type cells (Fig. 6E), probably because of a slower S-phase progression (see Fig. 3C). Importantly, the additional partial inactivation of the checkpoint (*slx4-S486A ddc1-T602A*) (Fig. 6E,F) allowed Cdc5-dependent Mms4 phosphorylation to occur earlier. Concomitantly, the binding of Mms4 to Dpb11 and Slx4 was rescued by partial checkpoint inactivation when immunoprecipitations were performed during the recovery phase (Fig. 6F). The occurrence of Mms4 phosphorylation

in the two mutants inversely correlated with DNA damage checkpoint activation (Rad53 phosphorylation) (Fig. 6E). It needs to be emphasized that Slx4–Dpb11 interaction is reduced, but not abolished, in the *slx4-S486A* mutant (Figs. 1B, 3A). The results in Figure 6, E and F, therefore suggest that the Slx4–Dpb11–Mms4–Mus81 complex can form earlier and potentially to a larger extent in the *slx4-S486A ddc1-T602A* mutant compared with the *slx4-S486A* single mutant. This offers a straightforward explanation for the rescue of the *slx4-S486A* mutant phenotypes by partial inactivation of the DNA damage checkpoint.

Taken together, we therefore identified an intricate regulatory mechanism of the Mus81 endonuclease, which critically depends on the formation of an Slx4–Dpb11–Mms4–Mus81 complex. The formation of this complex is activated by cell cycle stage-specific signaling and antagonized by the DNA damage checkpoint. Remarkably, complex formation and the direct control of Mus81 catalytic activity occur with similar timing, at the G2/M transition (Fig. 7).

Discussion

In this study, we describe a new facet of JM resolution following the bypass of DNA damage via template switch recombination. We describe a multiprotein complex containing Slx4, Dpb11, and Mus81–Mms4. This complex is cell cycle-controlled by at least two mechanisms: Cdk1-dependent phosphorylation of Slx4 and Cdc5-dependent phosphorylation of Mms4, and Dpb11 acts as a reader of both modifications. The conservation of the Slx4–Dpb11/TopBP1 interaction and its cell cycle regulation suggests that a similar complex may be involved in JM resolution in human cells. Importantly, the inhibition of Slx4 binding to Dpb11 causes phenotypes that are indicative of JM resolution defects, and we therefore infer that the association with Slx4 and Dpb11 promotes Mus81 function.

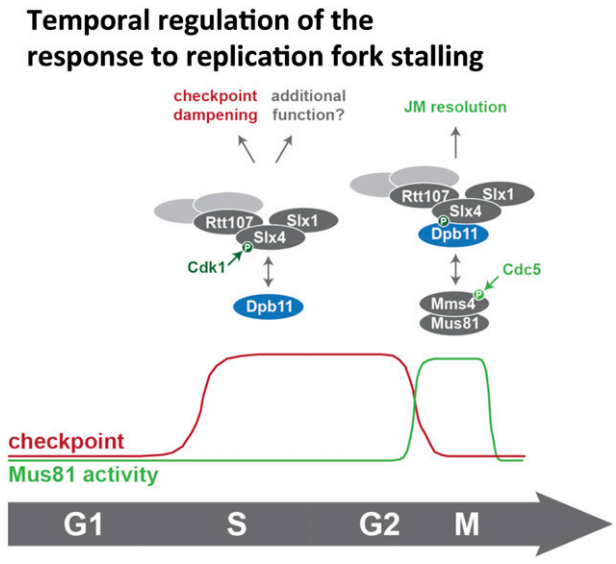

Figure 7. Model of the temporal response to replication fork stalling and its regulation by Slx4–Dpb11 complexes.

Slx4–Dpb11 multiprotein complex formation correlates with DNA JM resolution

The starting point of our analysis was a multiprotein complex containing Slx4, Dpb11, Slx1, and Rtt107 (Ohouo et al. 2010, 2012). In order to characterize a putative function of this complex in DNA repair, we tested whether the Slx4–Dpb11 complex would transiently interact with DNA repair enzymes and found an interaction with the Mus81–Mms4 structure-specific endonuclease specifically in mitotic cells. Based on the findings that the *slx4-S486A* mutant impairs complex formation and results in JM resolution defects, we propose that the Slx4–Dpb11 complex regulates Mus81–Mms4 activity. Our binding studies furthermore indicate a direct Dpb11–Mms4 interaction. Given the nature of Dpb11 as a scaffold protein, it appears likely that Dpb11 operates by tethering Mus81 to other activities that collaborate in the resolution reaction or targeting Mus81 to JM structures.

An intricate feature of the Slx4–Dpb11 complex is its complexity, as it involves four scaffold proteins: Dpb11, Slx4, Rtt107, and Mms4. An obvious advantage of such a multiscaffold complex is that its formation depends on several interaction surfaces, which offer numerous possibilities for regulation. The assembly of the complex therefore allows the integration of different cellular signals (for example, cell cycle and DNA damage), or one specific signal may control complex assembly by several mechanisms. Such a setup includes features of multisite phosphorylation systems, which have the ability to create switch-like transitions (Nash et al. 2001). Moreover, a multiscaffold complex may allow the assembly and coordination of different enzymatic activities (see below).

Our work has identified Mus81 as one catalytically active component of the Slx4–Dpb11 complex; a second one could potentially be Slx1. Recently, the Mus81 and Slx1 endonucleases from humans and mice have been shown to cooperate in the resolution of Holliday junctions in an Slx4-dependent manner (Wyatt et al. 2013). While our results suggest that also in budding yeast, Mus81 and Slx1 may be part of the same complex, we did not observe any specific defects in the response to MMS-induced replication fork stalling for *slx1Δ* cells (Supplemental Fig. S6D). Therefore, we conclude that either Slx1 is not involved in Mus81-dependent JM resolution in budding yeast or a functionally redundant nuclease compensates for the defects of the *slx1Δ* mutant.

Cell cycle regulation of the response to replication fork stalling and JM resolution

The cellular response to replication fork-stalling DNA lesions is intimately linked to the progression of the cell cycle. First, the primary problem, fork stalling, arises specifically in S phase. Moreover, the cells are required to finish the repair/bypass process at the latest in mitosis, when sister chromatids need to be accurately separated, and any remaining links between the chromatids have to be resolved.

In this study, we characterized two Dpb11 interactors: Slx4 and Mms4. Both proteins are phosphorylation tar-

gets of CDKs; however, Mms4 is additionally phosphorylated by the Polo-like kinase Cdc5 (Matos et al. 2011; Gallo-Fernández et al. 2012; Szakal and Branzei 2013). Interestingly, the Slx4–Dpb11 and Mms4–Dpb11 interactions display distinct cell cycle specificities: We observed a strong Slx4–Dpb11 interaction in asynchronous cultures as well as in S-phase and mitotic cells (Figs. 1C, 2C), while the Mms4–Dpb11 interaction was highly specific for mitosis (Fig. 5A). Accordingly, we found that the Mms4–Dpb11 interaction requires Cdc5, suggesting that Dpb11 can act as a reader of phosphorylation events that are initiated by different cell cycle kinases.

The cell cycle regulation of the Mus81–Mms4 association with the Slx4–Dpb11 complex correlates exactly with the known activity profile of Mus81 (Matos et al. 2011). Notably, the multiprotein complex is not the only mechanism of cell cycle regulation: Our in vitro resolution assays suggest that Cdc5 phosphorylation of Mus81–Mms4 directly stimulates Mus81 independently of complex formation. Therefore, we conclude that at least two parallel pathways of cell cycle regulation exist that promote appropriate Mus81 function in mitosis.

To date, it remains uncertain why cells restrict the activity of Mus81 until mitosis. The temporal regulation of Mus81 channels a large proportion of JMs into the Sgs1–Top3–Rmi1 dissolution pathway (Matos et al. 2011; Szakal and Branzei 2013). It has therefore been speculated that Sgs1-dependent dissolution, which leads to a NCO outcome (Ira et al. 2003), may be beneficial for cells dividing by a mitotic cell cycle. A second reason for restricting Mus81 activity may be the necessity to achieve temporal separation of the lesion bypass reaction and the JM resolution reaction (Saugar et al. 2013). Mus81 could impede the bypass reaction, given its relatively broad substrate specificity to a range of DNA structures (e.g., replication forks, D-loop structures, and Holliday junctions).

Intriguingly, the differences in the temporal regulation of the Slx4–Dpb11 and Mms4–Dpb11 interactions suggest that the composition of the Slx4–Dpb11 complex changes from the replication-associated template switch to the resolution reaction. Supporting the idea of several distinct Slx4–Dpb11 complexes is the fact that not all features of the Slx4–Dpb11 interaction (for example, enhanced binding after DNA damage) are seen in the Slx4–Dpb11–Mms4–Mus81 complex. It therefore appears plausible that Slx4–Dpb11 may associate with stalled replication forks already in S phase, while Mus81–Mms4 joins the complex in mitosis. It is tempting to speculate that the Slx4–Dpb11 complex may chaperone the DNA lesion site/repair intermediates until resolution (Fig. 7).

Regulation of JM resolution by the DNA damage checkpoint

The DNA damage checkpoint antagonizes JM resolution by Mus81 (Fig. 6; Szakal and Branzei 2013), and it has been suggested that Slx4 may act as negative regulator ("dampener") of the checkpoint by competing with binding of the checkpoint mediator Rad9 to Dpb11 (Ohouo et al. 2012). The JM resolution phenotypes of the *slx4-S486A* mutant could therefore, in principle, be explained by an indirect effect arising from checkpoint hyperactivation. Given the extensive ties between checkpoint and DNA repair pathways, the presented in vivo experiments cannot rule out a contribution of checkpoint misregulation to the observed JM resolution phenotypes.

We favor, however, a more direct role of Slx4 and Dpb11 in JM resolution for two reasons. First, the formation of the Slx4–Dpb11–Mms4–Mus81 complex and its regulation correlate with the temporal activation of Mus81. Second, the "dampener" model cannot account for all observed phenotypes. For example, the rescue of the MMS hypersensitivity of the *slx4-S486A* mutant by a covalent fusion with Dpb11 cannot be explained by competition, since in the fusion mutant, cells express two copies of full-length Dpb11 (one endogenous, one fused to Slx4), and therefore even more Dpb11 molecules (not less) are able to engage in checkpoint signaling complexes. Moreover, our analysis of RPA foci suggests that DNA lesions or repair intermediates persist and accumulate in the absence of a functional Slx4–Dpb11 complex, indicative of a role for Slx4 and Dpb11 in DNA repair.

Importantly, we found that the checkpoint regulates the formation of the Slx4–Dpb11–Mms4–Mus81 complex: Partial inhibition of the checkpoint enables Cdc5-dependent hyperphosphorylation of Mms4, which allows Dpb11 binding to occur earlier during the recovery from an MMS pulse and thereby reverses the effect of the *slx4* mutant. These findings suggest that at least in the *slx4-S486A* mutant background, the DNA damage checkpoint antagonizes the Slx4–Dpb11–Mms4–Mus81 complex. Partial inactivation of the checkpoint may therefore extend the temporal window during which Mus81 is active, which we propose to be beneficial in mutants with reduced JM resolution activity such as *slx4-S486A*. Whether this inhibitory mechanism takes place on the level of Cdc5 regulation in general (Zhang et al. 2009; Matos et al. 2013) or by specifically regulating Mms4 phosphorylation by Cdc5 remains to be determined. The important implication of this finding is that the activation of Mus81 is temporally restricted by two pathways: activation by cell cycle kinases and inhibition by the DNA damage checkpoint.

The Slx4–Dpb11 complex is conserved among eukaryotes

In addition to the mechanistic studies of the budding yeast Slx4–Dpb11 complex, we also provide the first evidence that at least parts of this complex may be found in human cells as well, since Slx4 and TopBP1 interact in a manner that depends on CDK phosphorylation of Slx4. It is worth noting that not all aspects of the protein network that controls resolution of JMs are conserved through evolution: While in human cells, Slx4 binds directly to Mus81–Eme1, this interaction appears to be absent in budding yeast (Fekairi et al. 2009; Muñoz et al. 2009; Svendsen et al. 2009; Schwartz et al. 2012). Given that both Slx4 and Mms4 bind to Dpb11, our data suggest that Dpb11 may serve as a bridge between the two proteins. Although a direct interaction between Slx4 and Mus81–Mms4 cannot be definitively

excluded, it appears as if the bridging interaction with Dpb11 in yeast may replace the direct interaction of Slx4 and Mus81 in human cells. Importantly, similar to our results in yeast, a stimulation of Slx4 binding to Mus81–Eme1 after phosphorylation by CDK and Polo-like kinase was observed in mitotic human cells as well (Wyatt et al. 2013). At this point, it seems therefore very likely that in both systems, JM resolution is promoted by a cell cycle-regulated complex containing several scaffold proteins.

Materials and methods

Yeast strains

All yeast strains are based on W303. Genotypes are listed in Supplemental Material.

Interaction assays

Coimmunoprecipitations of yeast extracts were performed using anti-Flag agarose resin (Sigma). Bound proteins were eluted with 3× Flag-peptide (Sigma).

For GST pull-downs, GST-Dpb11 or GST-tagged protein fragments were recombinantly expressed and purified as described (Pfander and Diffley 2011). Pull-downs were performed with ammonium sulphate-precipitated (57%) yeast extracts on glutathione sepharose 4B (GE Healthcare).

For coimmunoprecipitations from HEK293T, GFP-tagged proteins were transiently overexpressed and precipitated using GFP-Trap magnetic beads (Chromotek).

Nuclease activity assays

Nuclease assays on $Mms4^{3Flag}$ immunoprecipitations were done as described (Matos et al. 2011).

DNA gel electrophoresis

PFGE and 2D gel analysis of DNA intermediates were performed as previously described (Karras and Jentsch 2010; Szakal and Branzei 2013).

Mutation and recombination assays

Mutation rates were determined using a *CAN1* forward mutation assay. Interchromosomal recombination rates were determined using a direct repeat system using *leu2* heteroalleles (Aguilera and Klein 1988). CO rates were determined using a system harboring two *arg4* alleles on chromosome V and VIII (Robert et al. 2006; Szakal and Branzei 2013). In all, rates were determined by fluctuation analysis using a maximum likelihood approximation (Pfander et al. 2005).

Microscopy and immunofluorescence

Microscopy experiments were carried out as described (Germann et al. 2014).

A detailed methods description is provided in the Supplemental Material.

Acknowledgments

We thank U. Kagerer for excellent technical assistance, and C. Biertümpfel, J. Diffley, and H. Klein for providing plasmids, strains, and antibodies. We are grateful to Z. Storchova for help with microscopy analysis of RPA foci and thank S. Jentsch, M. Räschle, Z. Storchova, and members of the Jentsch and Pfander laboratories for stimulating discussion and critical reading of the manuscript. We thank the Max-Planck Institute of Biochemistry core facility for MS analysis. This work was supported by the Max-Planck Society and the German Research Council (Deutsche Forschungsgemeinschaft) to B.P.; the European Research Council, the Italian Association for International Cancer Research, and The Italian Foundation for Cancer Research (FIRC) to D.B.; and the Danish Agency for Science, Technology, and Innovation, the Villum Kann Rasmussen Foundation, the Lundbeck Foundation, and the European Research Council to M.L. S.C.S.B. is supported by a fellowship from the German Chemical Industry Association (VCI). B.S and D.B. performed the 2D gel experiments of Figure 4A and Supplemental Figure S6A–C and analyzed the data. M.L. performed the imaging experiments of Figure 4E and Supplemental Figure S7 and analyzed the data. J.M. performed the in vitro nuclease assays of Figure 5E and Supplemental Figure S9E and analyzed the data. B.H.H. did the bioinformatics analysis of Supplemental Figure S2. All other experiments were performed and analyzed by D.G., L.N.P., S.C.S.B, L.W., S.S., and B.P. B.P. wrote the paper, and all authors commented on the manuscript.

References

Aguilera A, Klein HL. 1988. Genetic control of intrachromosomal recombination in *Saccharomyces cerevisiae*. I. Isolation and genetic characterization of hyper-recombination mutations. *Genetics* **119:** 779–790.

Bishop AC, Ubersax JA, Petsch DT, Matheos DP, Gray NS, Blethrow J, Shimizu E, Tsien JZ, Schultz PG, Rose MD, et al. 2000. A chemical switch for inhibitor-sensitive alleles of any protein kinase. *Nature* **407:** 395–401.

Blanco MG, Matos J, Rass U, Ip SCY, West SC. 2010. Functional overlap between the structure-specific nucleases Yen1 and Mus81–Mms4 for DNA-damage repair in *S. cerevisiae*. *DNA Repair (Amst)* **9:** 394–402.

Branzei D, Foiani M. 2010. Maintaining genome stability at the replication fork. *Nat Rev Mol Cell Biol* **11:** 208–219.

Branzei D, Vanoli F, Foiani M. 2008. SUMOylation regulates Rad18-mediated template switch. *Nature* **456:** 915–920.

Cejka P, Plank JL, Bachrati CZ, Hickson ID, Kowalczykowski SC. 2010. Rmi1 stimulates decatenation of double Holliday junctions during dissolution by Sgs1–Top3. *Nat Struct Mol Biol* **17:** 1377–1382.

Chan K-L, North PS, Hickson ID. 2007. BLM is required for faithful chromosome segregation and its localization defines a class of ultrafine anaphase bridges. *EMBO J* **26:** 3397–3409.

Cordon-Preciado V, Ufano S, Bueno A. 2006. Limiting amounts of budding yeast Rad53 S-phase checkpoint activity results in increased resistance to DNA alkylation damage. *Nucleic Acids Res* **34:** 5852–5862.

Coulon S. 2006. Rad22Rad52-dependent repair of ribosomal DNA repeats cleaved by Slx1–Slx4 endonuclease. *Mol Biol Cell* **17:** 2081–2090.

Fekairi S, Scaglione S, Chahwan C, Taylor ER, Tissier A, Coulon S, Dong M-Q, Ruse C, Yates JR, Russell P, et al. 2009. Human SLX4 is a Holliday junction resolvase subunit that binds multiple DNA repair/recombination endonucleases. *Cell* **138:** 78–89.

Flott S, Alabert C, Toh GW, Toth R, Sugawara N, Campbell DG, Haber JE, Pasero P, Rouse J. 2007. Phosphorylation of Slx4 by Mec1 and Tel1 regulates the single-strand annealing mode of DNA repair in budding yeast. *Mol Cell Biol* **27:** 6433–6445.

Fricke WM, Brill SJ. 2003. Slx1–Slx4 is a second structure-specific endonuclease functionally redundant with Sgs1–Top3. *Genes Dev* **17:** 1768–1778.

Gaillard P-HL, Noguchi E, Shanahan P, Russell P. 2003. The endogenous Mus81–Eme1 complex resolves Holliday junctions by a nick and counternick mechanism. *Mol Cell* **12:** 747–759.

Gallo-Fernández M, Saugar I, Ortiz-Bazán MÁ, Vázquez MV, Tercero JA. 2012. Cell cycle-dependent regulation of the nuclease activity of Mus81–Eme1/Mms4. *Nucleic Acids Res* **40:** 8325–8335.

Garcia V, Furuya K, Carr AM. 2005. Identification and functional analysis of TopBP1 and its homologs. *DNA Repair (Amst)* **4:** 1227–1239.

Germann SM, Oestergaard VH, Haas C, Salis P, Motegi A, Lisby M. 2011. Dpb11/TopBP1 plays distinct roles in DNA replication, checkpoint response and homologous recombination. *DNA Repair (Amst)* **10:** 210–224.

Germann SM, Schramke V, Pedersen RT, Gallina I, Eckert-Boulet N, Oestergaard VH, Lisby M. 2014. TopBP1/Dpb11 binds DNA anaphase bridges to prevent genome instability. *J Cell Biol* **204:** 45–59.

Giannattasio M, Lazzaro F, Plevani P, Muzi-Falconi M. 2005. The DNA damage checkpoint response requires histone H2B ubiquitination by Rad6–Bre1 and H3 methylation by Dot1. *J Biol Chem* **280:** 9879–9886.

Harrison JC, Haber JE. 2006. Surviving the breakup: the DNA damage checkpoint. *Annu Rev Genet* **40:** 209–235.

Ho CK, Mazón G, Lam AF, Symington LS. 2010. Mus81 and Yen1 promote reciprocal exchange during mitotic recombination to maintain genome integrity in budding yeast. *Mol Cell* **40:** 988–1000.

Holt LJ, Tuch BB, Villén J, Johnson AD, Gygi SP, Morgan DO. 2009. Global analysis of Cdk1 substrate phosphorylation sites provides insights into evolution. *Science* **325:** 1682–1686.

Interthal H, Heyer WD. 2000. MUS81 encodes a novel helix–hairpin–helix protein involved in the response to UV- and methylation-induced DNA damage in *Saccharomyces cerevisiae*. *Mol Gen Genet* **263:** 812–827.

Ip SCY, Rass U, Blanco MG, Flynn HR, Skehel JM, West SC. 2008. Identification of Holliday junction resolvases from humans and yeast. *Nature* **456:** 357–361.

Ira G, Malkova A, Liberi G, Foiani M, Haber JE. 2003. Srs2 and Sgs1–Top3 suppress crossovers during double-strand break repair in yeast. *Cell* **115:** 401–411.

Karras GI, Jentsch S. 2010. The RAD6 DNA damage tolerance pathway operates uncoupled from the replication fork and is functional beyond S phase. *Cell* **141:** 255–267.

Li M, Brill SJ. 2005. Roles of SGS1, MUS81, and RAD51 in the repair of lagging-strand replication defects in *Saccharomyces cerevisiae*. *Curr Genet* **48:** 213–225.

Liberi G, Maffioletti G, Lucca C, Chiolo I, Baryshnikova A, Cotta-Ramusino C, Lopes M, Pellicioli A, Haber JE, Foiani M. 2005. Rad51-dependent DNA structures accumulate at damaged replication forks in sgs1 mutants defective in the yeast ortholog of BLM RecQ helicase. *Genes Dev* **19:** 339–350.

Mankouri HW, Ashton TM, Hickson ID. 2011. Holliday junction-containing DNA structures persist in cells lacking Sgs1 or Top3 following exposure to DNA damage. *Proc Natl Acad Sci* **108:** 4944–4949.

Mankouri HW, Huttner D, Hickson ID. 2013. How unfinished business from S-phase affects mitosis and beyond. *EMBO J* **32:** 2661–2671.

Matos J, Blanco MG, Maslen S, Skehel JM, West SC. 2011. Regulatory control of the resolution of DNA recombination intermediates during meiosis and mitosis. *Cell* **147:** 158–172.

Matos J, Blanco MG, West SC. 2013. Cell-cycle kinases coordinate the resolution of recombination intermediates with chromosome segregation. *Cell Rep* 1–11.

Mordes DA, Nam EA, Cortez D. 2008. Dpb11 activates the Mec1–Ddc2 complex. *Proc Natl Acad Sci* **105:** 18730–18734.

Mullen JR, Kaliraman V, Ibrahim SS, Brill SJ. 2001. Requirement for three novel protein complexes in the absence of the Sgs1 DNA helicase in *Saccharomyces cerevisiae*. *Genetics* **157:** 103–118.

Muñoz IM, Hain K, Déclais A-C, Gardiner M, Toh GW, Sanchez-Pulido L, Heuckmann JM, Toth R, Macartney T, Eppink B, et al. 2009. Coordination of structure-specific nucleases by human SLX4/BTBD12 is required for DNA repair. *Mol Cell* **35:** 116–127.

Nash P, Tang X, Orlicky S, Chen Q, Gertler FB, Mendenhall MD, Sicheri F, Pawson T, Tyers M. 2001. Multisite phosphorylation of a CDK inhibitor sets a threshold for the onset of DNA replication. *Nature* **414:** 514–521.

Navadgi-Patil VM, Burgers PM. 2008. Yeast DNA replication protein Dpb11 activates the Mec1/ATR checkpoint kinase. *J Biol Chem* **283:** 35853–35859.

Ohouo PY, Bastos de Oliveira FM, Almeida BS, Smolka MB. 2010. DNA damage signaling recruits the Rtt107–Slx4 scaffolds via Dpb11 to mediate replication stress response. *Mol Cell* **39:** 300–306.

Ohouo PY, de Oliveira FMB, Liu Y, Ma CJ, Smolka MB. 2012. DNA-repair scaffolds dampen checkpoint signalling by counteracting the adaptor Rad9. *Nature* **493:** 120–124.

Pfander B, Diffley JFX. 2011. Dpb11 coordinates Mec1 kinase activation with cell cycle-regulated Rad9 recruitment. *EMBO J* **30:** 4897–4907.

Pfander B, Moldovan GL, Sacher M, Hoege C, Jentsch S. 2005. SUMO-modified PCNA recruits Srs2 to prevent recombination during S phase. *Nature* **436:** 428–433.

Prakash S, Johnson RE, Prakash L. 2005. Eukaryotic translesion synthesis DNA polymerases: specificity of structure and function. *Annu Rev Biochem* **74:** 317–353.

Puddu F, Granata M, Di Nola L, Balestrini A, Piergiovanni G, Lazzaro F, Giannattasio M, Plevani P, Muzi-Falconi M. 2008. Phosphorylation of the budding yeast 9-1-1 complex is required for Dpb11 function in the full activation of the UV-induced DNA damage checkpoint. *Mol Cell Biol* **28:** 4782–4793.

Rappas M, Oliver AW, Pearl LH. 2011. Structure and function of the Rad9-binding region of the DNA-damage checkpoint adaptor TopBP1. *Nucleic Acids Res* **39:** 313–324.

Robert T, Dervins D, Fabre F, Gangloff S. 2006. Mrc1 and Srs2 are major actors in the regulation of spontaneous crossover. *EMBO J* **25:** 2837–2846.

Roberts TM, Kobor MS, Bastin-Shanower SA, Ii M, Horte SA, Gin JW, Emili A, Rine J, Brill SJ, Brown GW. 2006. Slx4 regulates DNA damage checkpoint-dependent phosphorylation of the BRCT domain protein Rtt107/Esc4. *Mol Biol Cell* **17:** 539–548.

Saugar I, Vazquez MV, Gallo-Fernandez M, Ortiz-Bazan MA, Segurado M, Calzada A, Tercero JA. 2013. Temporal regulation of the Mus81–Mms4 endonuclease ensures cell survival under conditions of DNA damage. *Nucleic Acids Res* **41:** 8943–8958.

Schwartz EK, Wright WD, Ehmsen KT, Evans JE, Stahlberg H, Heyer WD. 2012. Mus81–Mms4 functions as a single heterodimer to cleave nicked intermediates in recombinational DNA repair. *Mol Cell Biol* **32:** 3065–3080.

Snead JL, Sullivan M, Lowery DM, Cohen MS, Zhang C, Randle DH, Taunton J, Yaffe MB, Morgan DO, Shokat KM. 2007. A coupled chemical-genetic and bioinformatic approach to

Polo-like kinase pathway exploration. *Chem Biol* **14:** 1261–1272.

Svendsen JM, Smogorzewska A, Sowa ME, O'Connell BC, Gygi SP, Elledge SJ, Harper JW. 2009. Mammalian BTBD12/SLX4 assembles a Holliday junction resolvase and is required for DNA repair. *Cell* **138:** 63–77.

Szakal B, Branzei D. 2013. Premature Cdk1/Cdc5/Mus81 pathway activation induces aberrant replication and deleterious crossover. *EMBO J* **32:** 1155–1167.

Tanaka S, Umemori T, Hirai K, Muramatsu S, Kamimura Y, Araki H. 2007. CDK-dependent phosphorylation of Sld2 and Sld3 initiates DNA replication in budding yeast. *Nature* **445:** 328–332.

Tomkinson AE, Bardwell AJ, Bardwell L, Tappe NJ, Friedberg EC. 1993. Yeast DNA repair and recombination proteins Rad1 and Rad10 constitute a single-stranded-DNA endonuclease. *Nature* **362:** 860–862.

Wyatt HDM, Sarbajna S, Matos J, West SC. 2013. Coordinated actions of SLX1–SLX4 and MUS81–EME1 for Holliday junction resolution in human cells. *Mol Cell* **52:** 234–247.

Yu X. 2003. The BRCT domain is a phospho-protein binding domain. *Science* **302:** 639–642.

Zegerman P, Diffley JFX. 2007. Phosphorylation of Sld2 and Sld3 by cyclin-dependent kinases promotes DNA replication in budding yeast. *Nature* **445:** 281–285.

Zhang T, Nirantar S, Lim HH, Sinha I, Surana U. 2009. DNA damage checkpoint maintains Cdh1 in an active state to inhibit anaphase progression. *Dev Cell* **17:** 541–551.

Supplemental Information – Outline

- Supplemental Figures
- Supplemental Figure Legends
- Supplemental Methods
- References

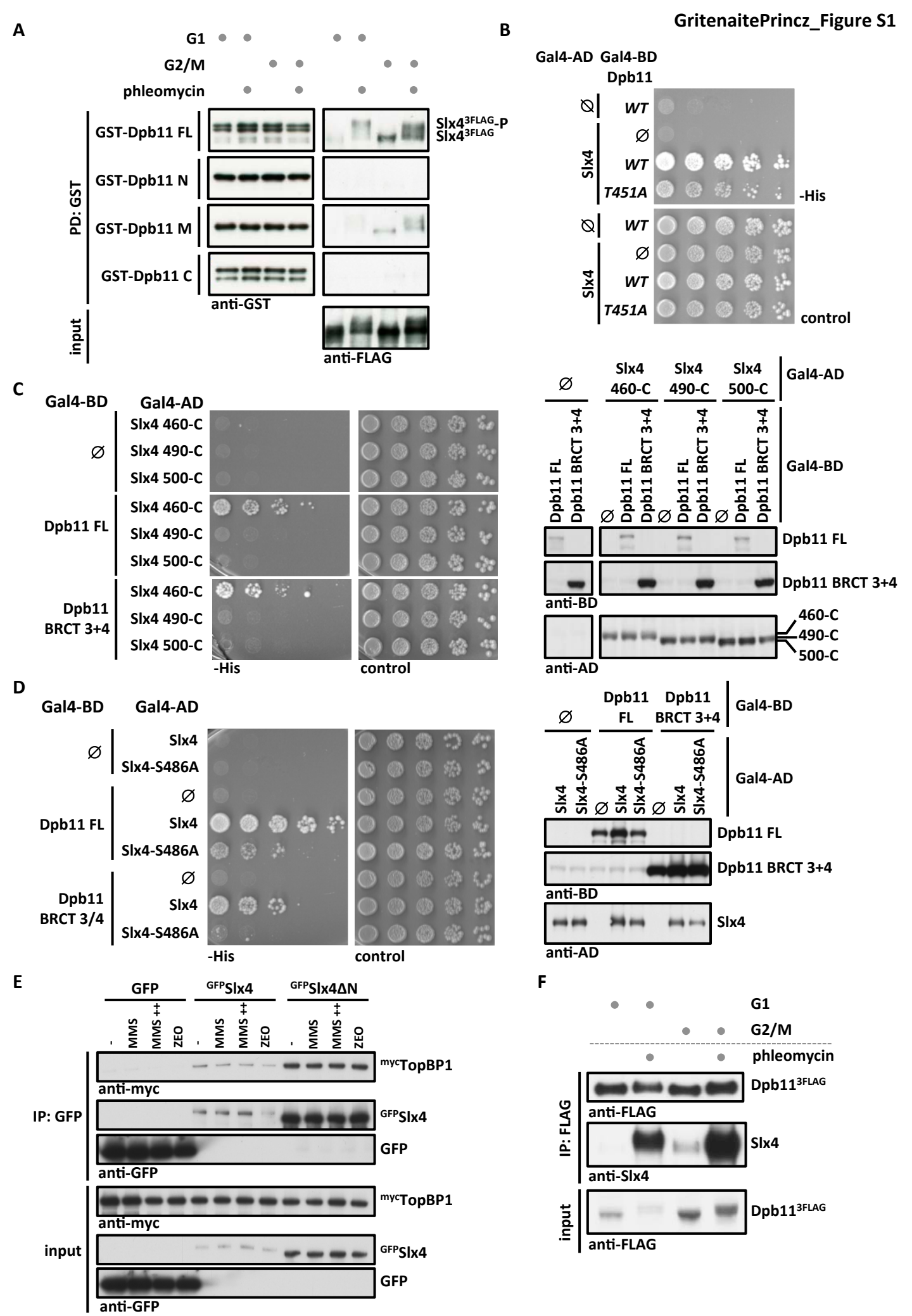
A
G1
G2/M
phleomycin
PD: GST
GST-Dpb11 FL
GST-Dpb11 N
GST-Dpb11 M
GST-Dpb11 C
anti-GST
input
anti-FLAG
Slx4^3FLAG-P
Slx4^3FLAG
B
Gal4-AD
Gal4-BD
Dpb11
Slx4
WT
T451A
-His
control
C
Gal4-BD
Gal4-AD
Slx4 460-C
Slx4 490-C
Slx4 500-C
Dpb11 FL
Dpb11 BRCT 3+4
-His
control
D
Gal4-BD
Gal4-AD
Slx4
Slx4-S486A
Dpb11 FL
Dpb11 BRCT 3/4
-His
control
E
GFP
GFPSlx4
GFPSlx4ΔN
-
MMS
MMS ++
ZEO
IP: GFP
anti-myc
anti-GFP
input
mycTopBP1
GFPSlx4
GFP
F
G1
G2/M
phleomycin
IP: FLAG
input
anti-FLAG
anti-Slx4
Dpb11^3FLAG
Slx4

Dpb11/TopBP1 interaction motif in Slx4 proteins from different eukaryotes

```
Sp   156 GFYYHR-----KPQLFEKSLEKLGNK---SIEA-NR---SPLIKELC 190
Sc   458 QFFTPN--TSPLDGIIDLTQE--------SFKA-VRSLISPLKVENN 493 (S486)
Kl   372 KTKREYSRANINDQLINISQT--------SYDV-VSSIVSPMKAQRT 409
Ec   347 PDESPDNLPIHEDTVIDLTQE--------TFRA-VSNIASPVKATSR 384
Nc   494 SQSPTPGTSPQQDEIIDLTQE--------SFKA-VGRLISPVRPPTL 531
Ka   374 SIFSAHPSPEKPDNIIDLSVG--------SFKA-VKSLVSPIKPDVV 411
Td   282 QFYTPR--TTPPDEIIDLTQE--------SFKV-VKSLISPLKD--- 314
Zr   305 DAGTPKTAHSPSDGVIDLTNG--------SFKV-VKSLISPLK---- 338
Vp   391 QFFTADG--NMVDGVIDLTQG--------SFKA-VTKLFSPLKVDTL 426
Lt   385 HTYRTPSGLAGRDQLIDLTQC--------SFNA-VKSLISPLKS--- 419
Hs  1236 WLFCDRESSPSEASTTDTSW---------LVPA-TP-LASRSRDCSS 1271 (T1260)
Sb  1196 WLFCDRESSPEEGSTTDTSW---------LVPA-TP-LAGRSRDCSS 1231
Mm  1038 WLLCSQKTSLDEDSATDTSW---------LVPA-TP-GVSRSRDCSS 1073
Rn  1242 WLFCSQTPSLGEDSATESSW---------LVPA-TP-GASKSRDRSS 1277
Sh  1214 RPVTRHE----ESSTTDTSW---------LVPA-TP-LTNRSHDCSS 1245
Tm  1250 QLFCKAESSP-EASTTDTSW---------LVPA-TP-LASRGCHRSS 1284
Oo  1244 QLFCDPKISGDEDSTTDTSW---------LVPA-TP-LASRSRDCSS 1279
Xt  1129 EVPQIST--IQSAFHYN-SLSPPL-----LSPAKSP-AKPLSPPVSP 1166
Dr  1168 DVSRASTMGHLAQGVPQPSSSTP------VHSVGS--LQRKILFDSP 1207
Dm   281 EGPIDDLESYYVTDLFEVSRTPAHHLLKNWAAI-QGRDFSPERETQK 326
Dg   283 EESLANLSAYYVQDLFEVSRTPAHHLLKNWAAI-QGRDLSPKRPSKE 328
Dw   276 EDPIELN-VYYVKDLIEISYTPAEHLLKDWSAI-QGRDLSPKRLNPK 320
Cc   325 DEHRANLDEFYVRSLFEVANVQAGYLLKDWHAI-EGRDKSPKHRPNK 370
Ag   343 LPSEQLMEMYYVPELLEANPAPVGCMLKDWSKI-PGRECTPERELDG 388
```

A

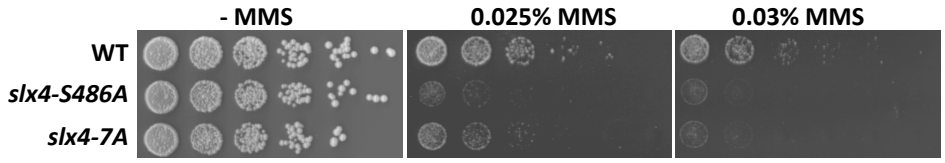
- MMS
0.025% MMS
0.03% MMS
WT
slx4-S486A
slx4-7A

B

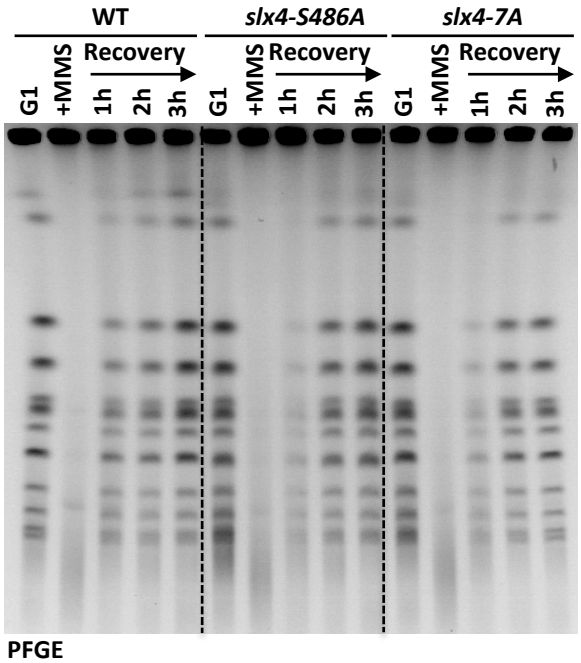
WT
slx4-S486A
slx4-7A
Recovery
G1
+MMS
1h
2h
3h
PFGE

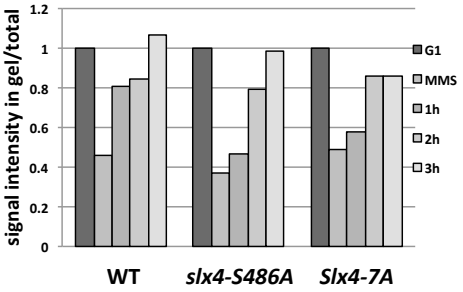
signal intensity in gel/total
1.2
1
0.8
0.6
0.4
0.2
0
G1
MMS
1h
2h
3h
WT
slx4-S486A
Slx4-7A

C

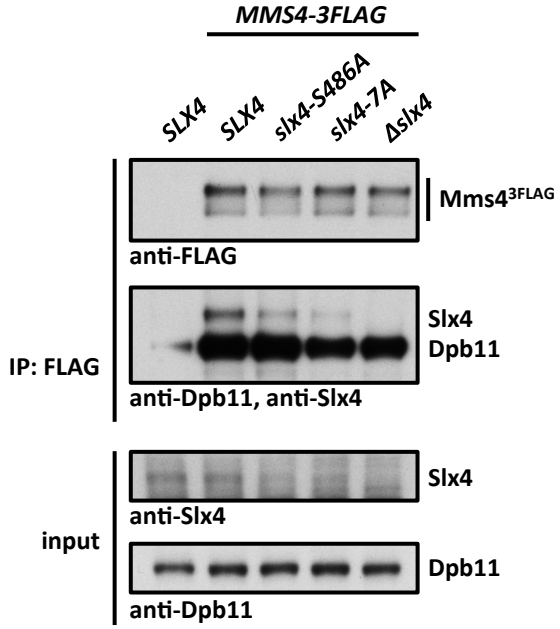
MMS4-3FLAG
SLX4
SLX4
slx4-S486A
slx4-7A
Δslx4
Mms4^3FLAG
anti-FLAG
IP: FLAG
Slx4
Dpb11
anti-Dpb11, anti-Slx4
input
Slx4
anti-Slx4
Dpb11
anti-Dpb11

A

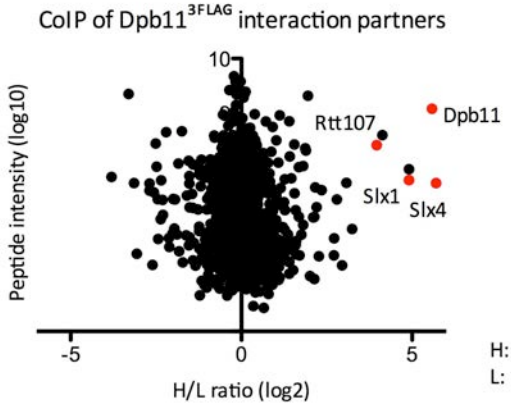

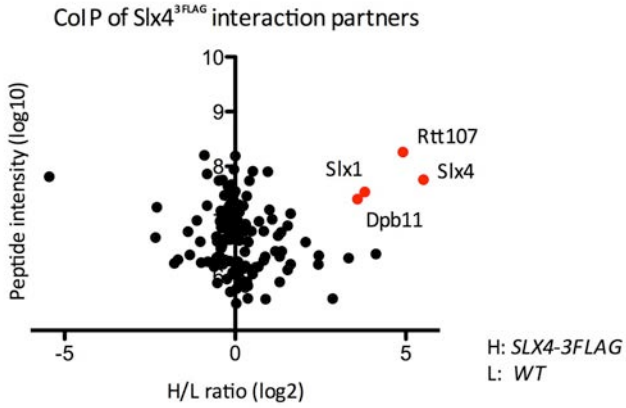

Best scoring MS-MS spectrum of SLX4 phospho-S486 peptide from Dpb11 3FLAG CoIP :

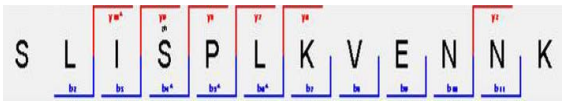

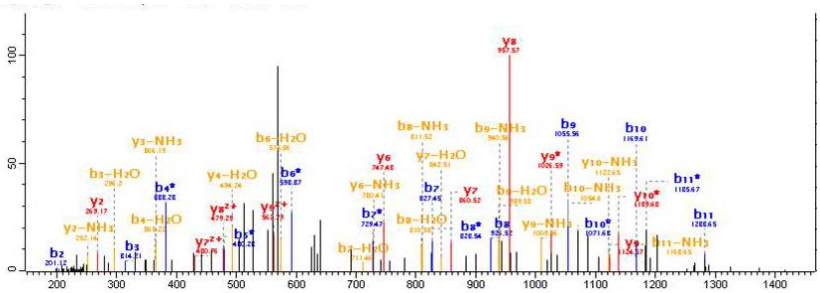

B

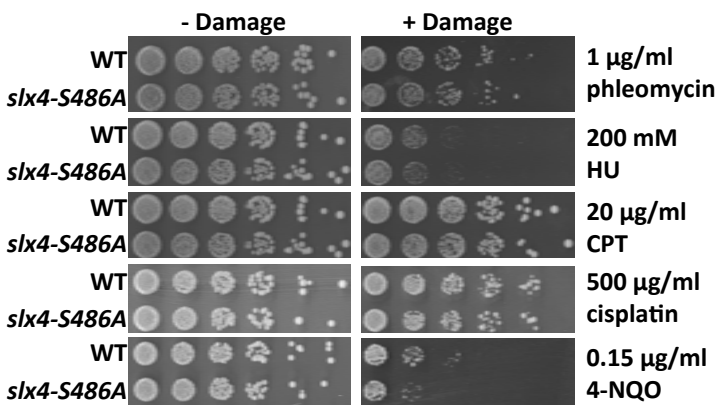

C

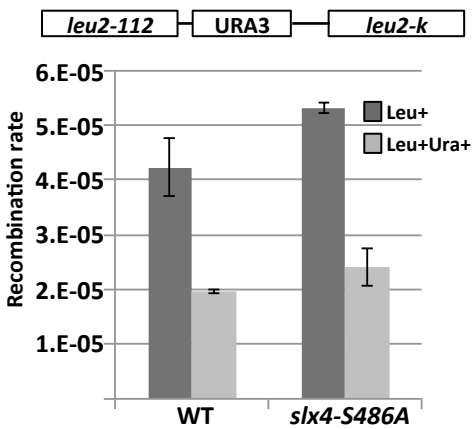

D

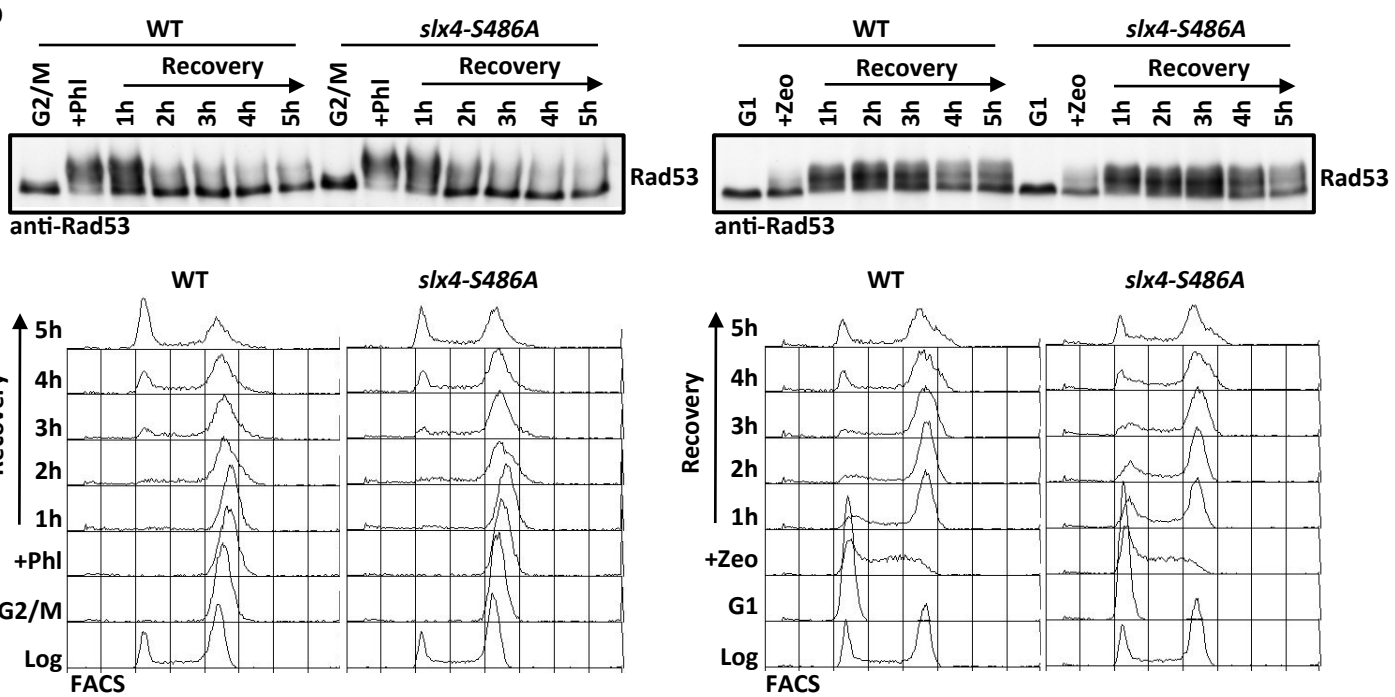

A

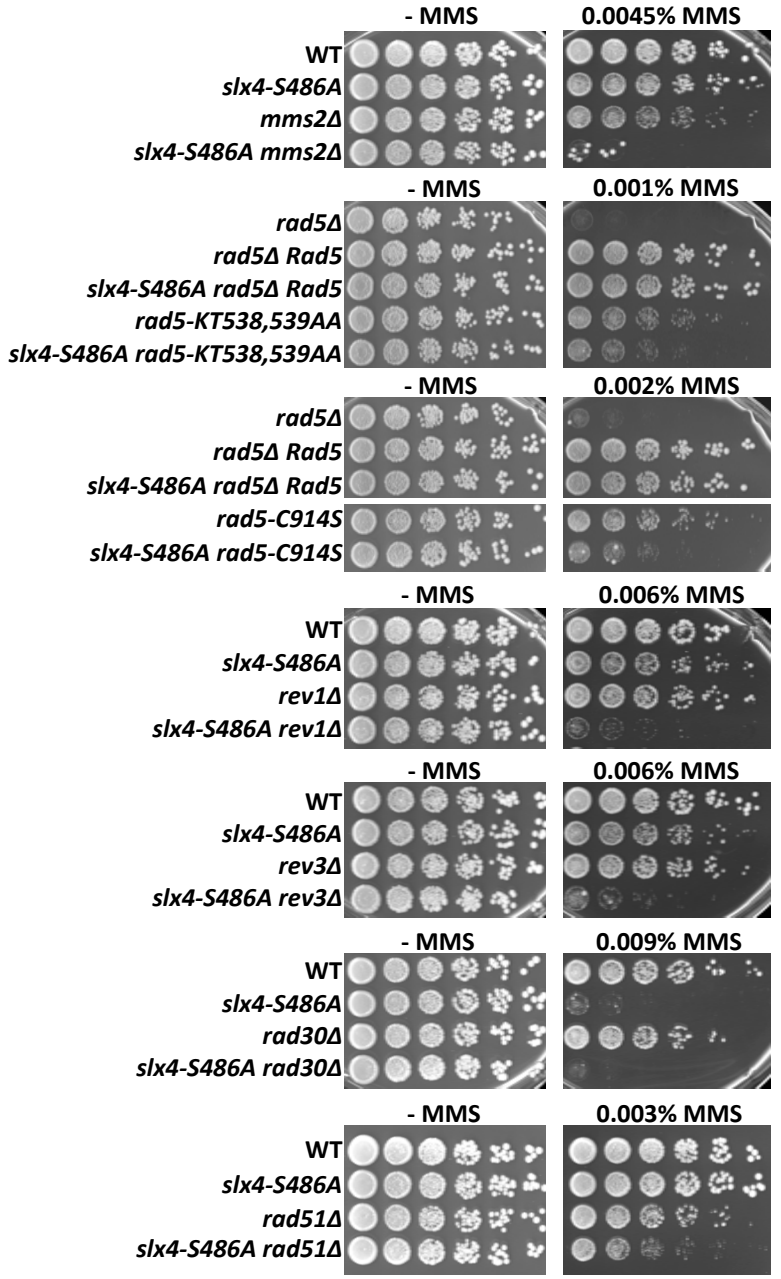
- MMS
0.0045% MMS
WT
slx4-S486A
mms2Δ
slx4-S486A mms2Δ
- MMS
0.001% MMS
rad5Δ
rad5Δ Rad5
slx4-S486A rad5Δ Rad5
rad5-KT538,539AA
slx4-S486A rad5-KT538,539AA
- MMS
0.002% MMS
rad5Δ
rad5Δ Rad5
slx4-S486A rad5Δ Rad5
rad5-C914S
slx4-S486A rad5-C914S
- MMS
0.006% MMS
WT
slx4-S486A
rev1Δ
slx4-S486A rev1Δ
- MMS
0.006% MMS
WT
slx4-S486A
rev3Δ
slx4-S486A rev3Δ
- MMS
0.009% MMS
WT
slx4-S486A
rad30Δ
slx4-S486A rad30Δ
- MMS
0.003% MMS
WT
slx4-S486A
rad51Δ
slx4-S486A rad51Δ

B

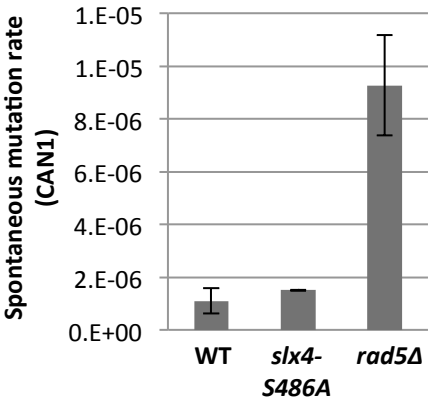
Spontaneous mutation rate (CAN1)
1.E-05
1.E-05
8.E-06
6.E-06
4.E-06
2.E-06
0.E+00
WT
slx4-S486A
rad5Δ

C

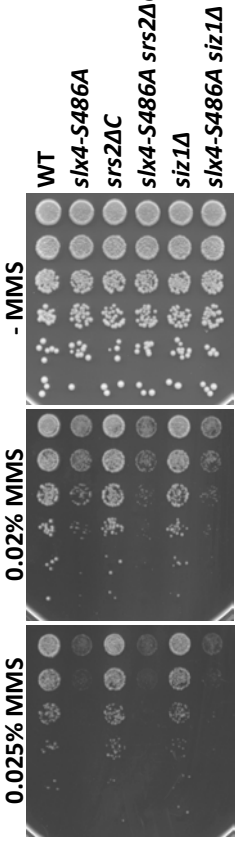
WT
slx4-S486A
srs2ΔC
slx4-S486A srs2ΔC
siz1Δ
slx4-S486A siz1Δ
- MMS
0.02% MMS
0.025% MMS

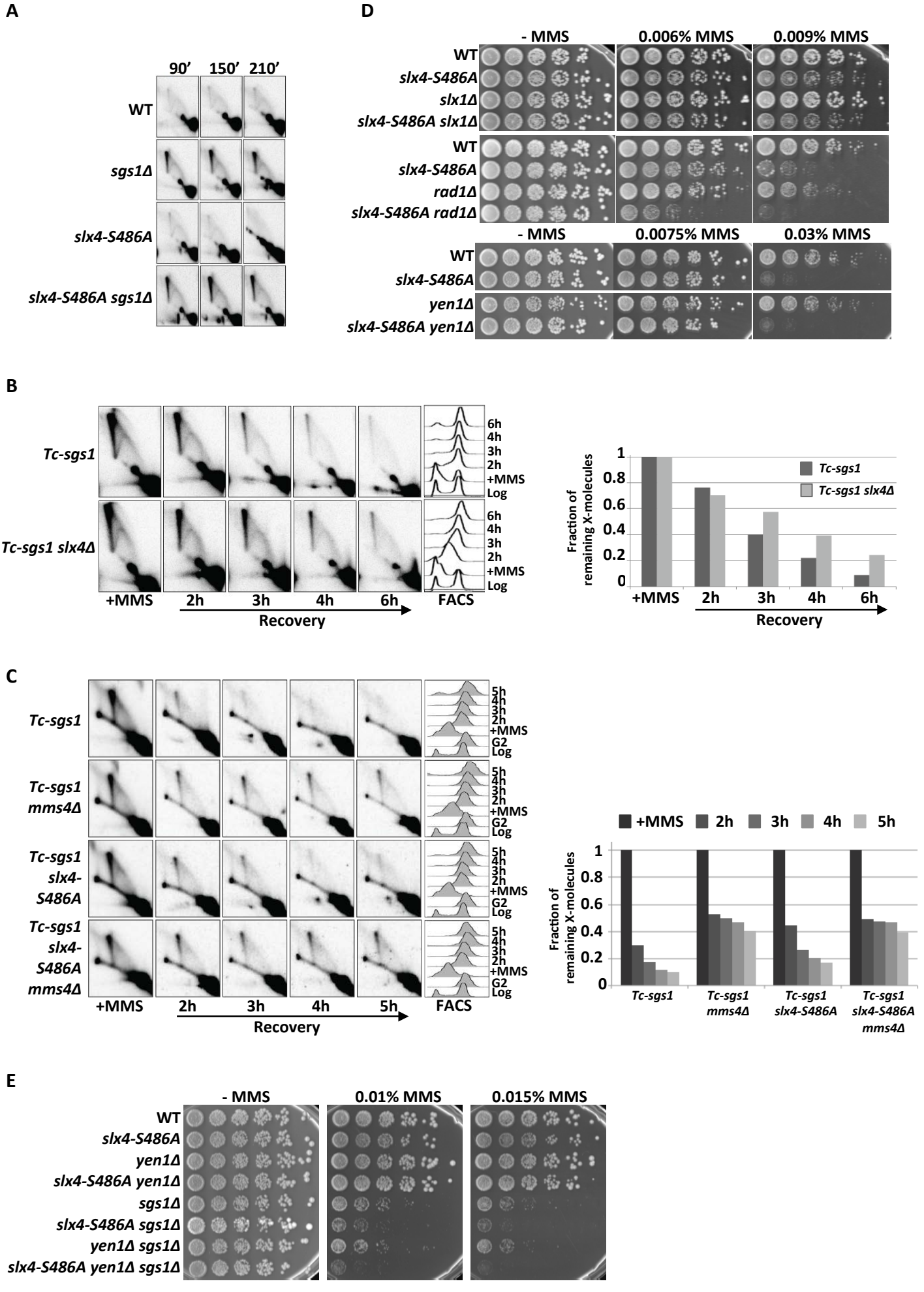
A
90'
150'
210'
WT
sgs1Δ
slx4-S486A
slx4-S486A sgs1Δ
D
- MMS
0.006% MMS
0.009% MMS
WT
slx4-S486A
slx1Δ
slx4-S486A slx1Δ
WT
slx4-S486A
rad1Δ
slx4-S486A rad1Δ
- MMS
0.0075% MMS
0.03% MMS
WT
slx4-S486A
yen1Δ
slx4-S486A yen1Δ
B
Tc-sgs1
Tc-sgs1 slx4Δ
6h
4h
3h
2h
+MMS
Log
FACS
+MMS
2h
3h
4h
6h
Recovery
Fraction of remaining X-molecules
Tc-sgs1
Tc-sgs1 slx4Δ
C
Tc-sgs1
Tc-sgs1 mms4Δ
Tc-sgs1 slx4-S486A
Tc-sgs1 slx4-S486A mms4Δ
5h
4h
3h
2h
+MMS
G2
Log
FACS
+MMS
2h
3h
4h
5h
Recovery
Fraction of remaining X-molecules
Tc-sgs1
Tc-sgs1 mms4Δ
Tc-sgs1 slx4-S486A
Tc-sgs1 slx4-S486A mms4Δ
E
- MMS
0.01% MMS
0.015% MMS
WT
slx4-S486A
yen1Δ
slx4-S486A yen1Δ
sgs1Δ
slx4-S486A sgs1Δ
yen1Δ sgs1Δ
slx4-S486A yen1Δ sgs1Δ

A

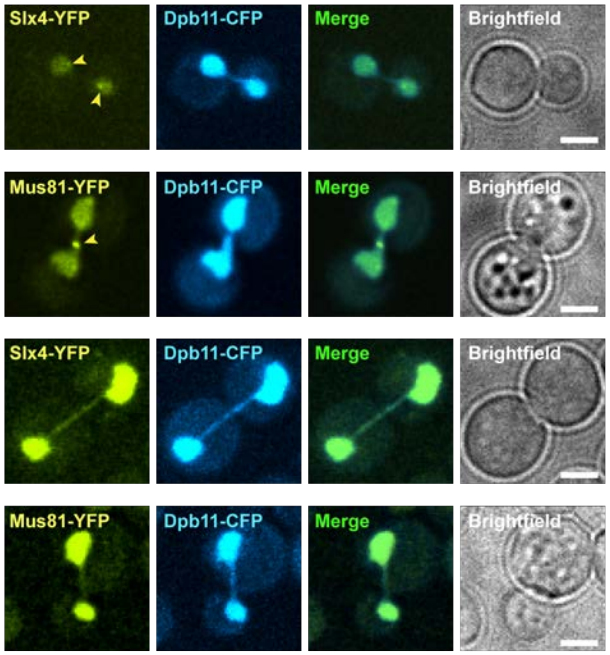
Slx4-YFP
Dpb11-CFP
Merge
Brightfield
Mus81-YFP
Dpb11-CFP
Merge
Brightfield
Slx4-YFP
Dpb11-CFP
Merge
Brightfield
Mus81-YFP
Dpb11-CFP
Merge
Brightfield

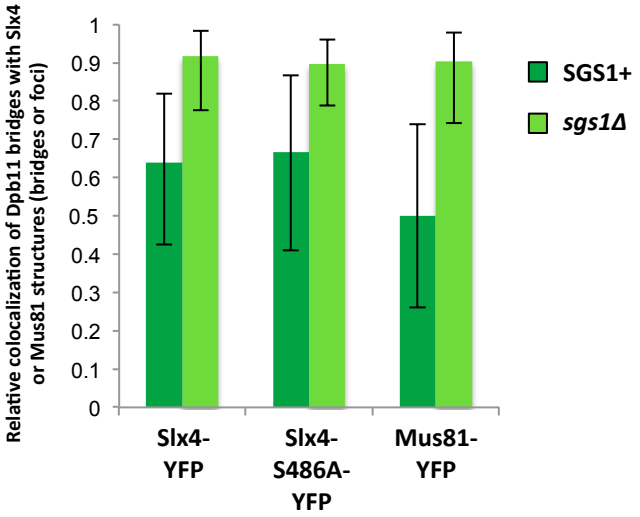
Relative colocalization of Dpb11 bridges with Slx4 or Mus81 structures (bridges or foci)
0
0.1
0.2
0.3
0.4
0.5
0.6
0.7
0.8
0.9
1
Slx4-YFP
Slx4-S486A-YFP
Mus81-YFP
SGS1+
sgs1Δ

B

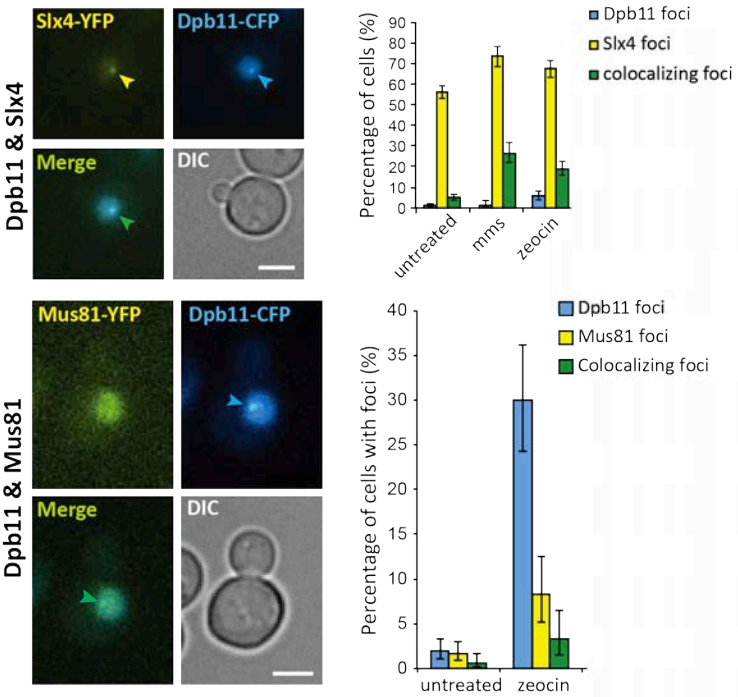
Dpb11 & Slx4
Slx4-YFP
Dpb11-CFP
Merge
DIC
Percentage of cells (%)
Dpb11 foci
Slx4 foci
colocalizing foci
untreated
mms
zeocin
Dpb11 & Mus81
Mus81-YFP
Dpb11-CFP
Merge
DIC
Percentage of cells with foci (%)
Dpb11 foci
Mus81 foci
Colocalizing foci
untreated
zeocin

A

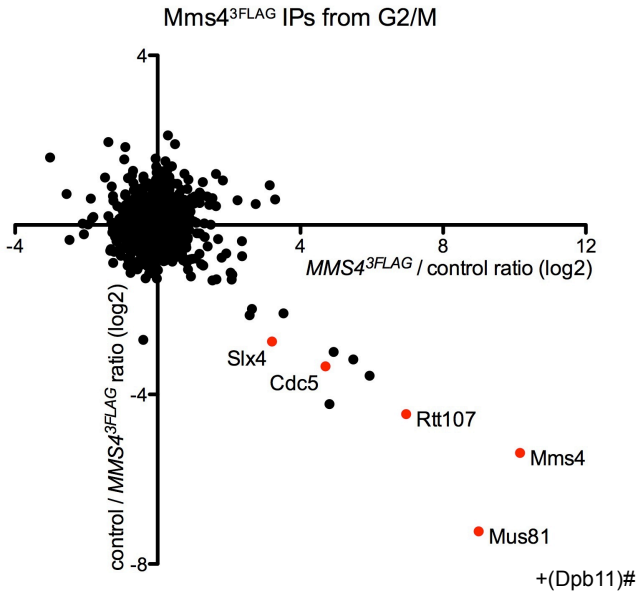
Mms4^3FLAG IPs from G2/M
MMS4^3FLAG / control ratio (log2)
control / MMS4^3FLAG ratio (log2)
Slx4
Cdc5
Rtt107
Mms4
Mus81
+(Dpb11)#

C

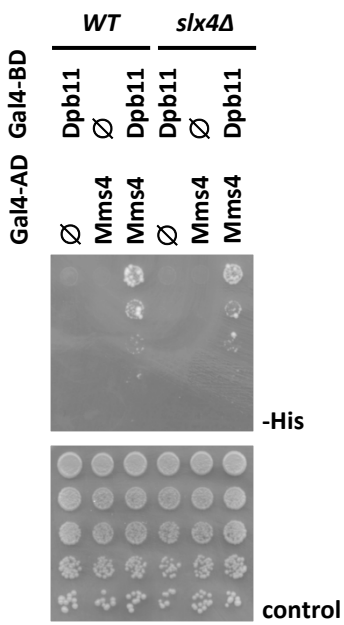
WT
slx4Δ
Gal4-BD
Dpb11
∅
Dpb11
Dpb11
∅
Dpb11
Gal4-AD
∅
Mms4
Mms4
∅
Mms4
Mms4
-His
control

B


glycerol gradient
10%
30%
input
1 2 3 4 5 6 7 8 9 10 11 12 13 14 15 16 17 18 19 20 21 22
Mms4^3FLAG
anti-FLAG
Slx4
Dpb11
anti-Dpb11,
anti-Slx4

D

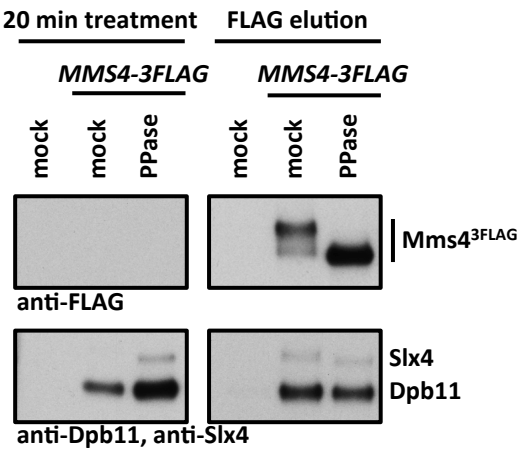
20 min treatment
FLAG elution
MMS4-3FLAG
MMS4-3FLAG
mock
mock
PPase
mock
mock
PPase
Mms4^3FLAG
anti-FLAG
Slx4
Dpb11
anti-Dpb11, anti-Slx4

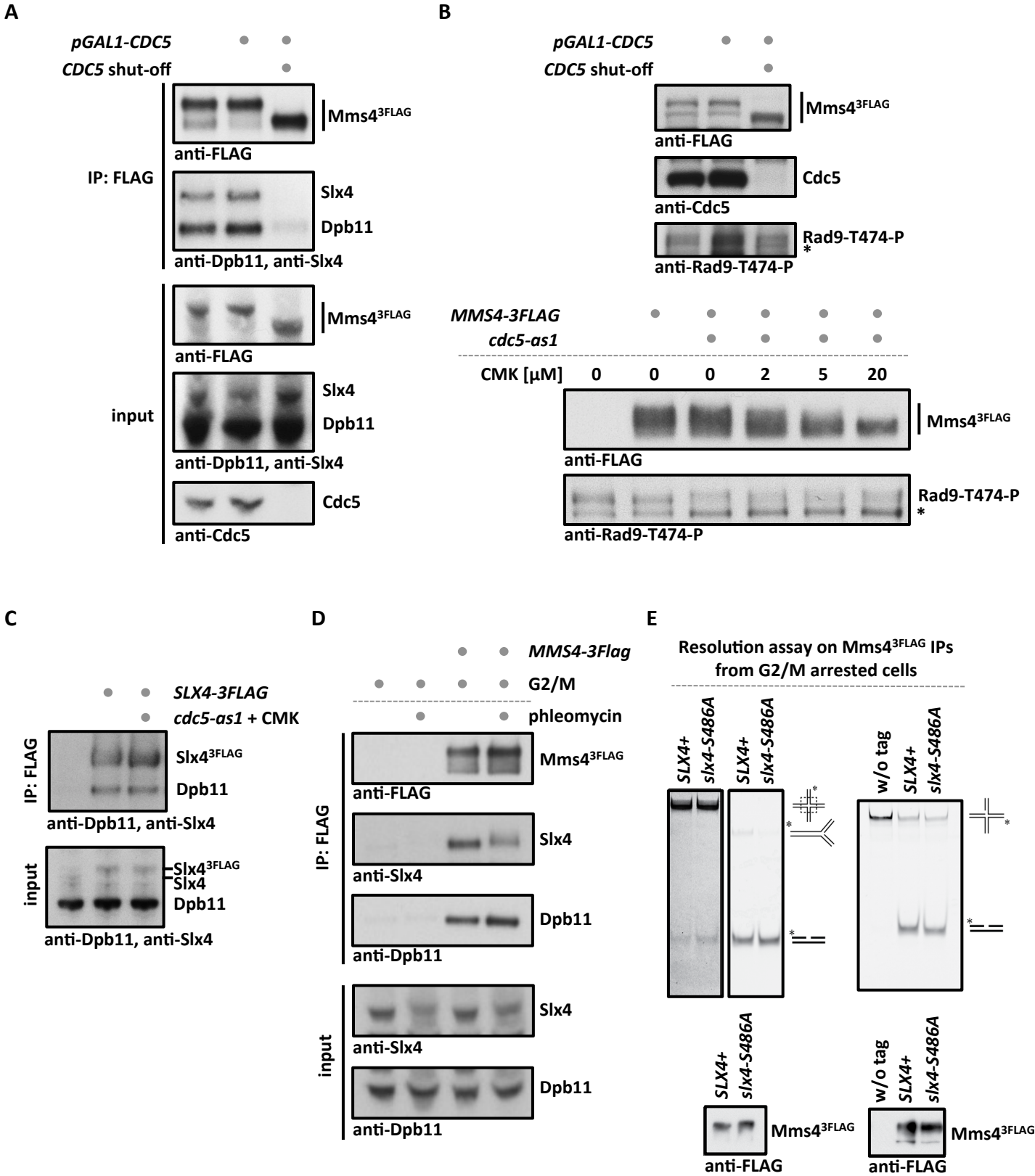
A
pGAL1-CDC5
CDC5 shut-off
Mms4^3FLAG
anti-FLAG
IP: FLAG
Slx4
Dpb11
anti-Dpb11, anti-Slx4
input
Cdc5
anti-Cdc5
B
pGAL1-CDC5
CDC5 shut-off
Mms4^3FLAG
anti-FLAG
Cdc5
anti-Cdc5
Rad9-T474-P
anti-Rad9-T474-P
MMS4-3FLAG
cdc5-as1
CMK [μM] 0 0 0 2 5 20
C
SLX4-3FLAG
cdc5-as1 + CMK
Slx4^3FLAG
Dpb11
Slx4
D
MMS4-3Flag
G2/M
phleomycin
E
Resolution assay on Mms4^3FLAG IPs from G2/M arrested cells
SLX4+
slx4-S486A
w/o tag

A

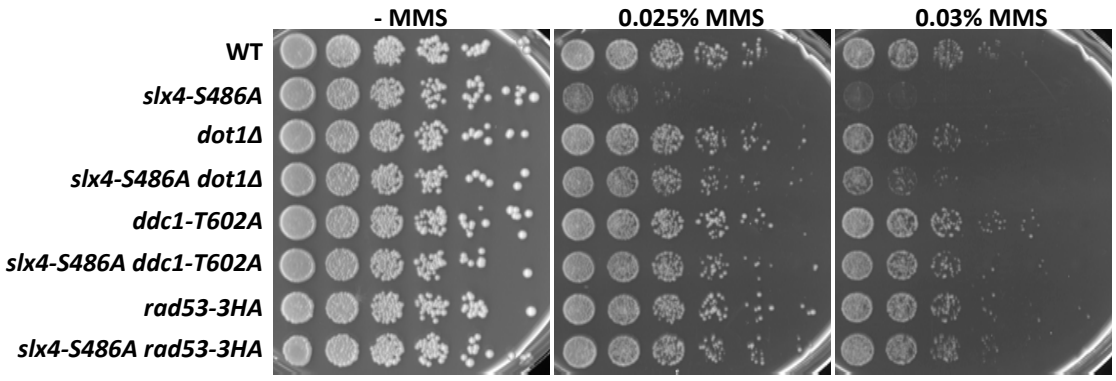
- MMS
0.025% MMS
0.03% MMS
WT
slx4-S486A
dot1Δ
slx4-S486A dot1Δ
ddc1-T602A
slx4-S486A ddc1-T602A
rad53-3HA
slx4-S486A rad53-3HA

B

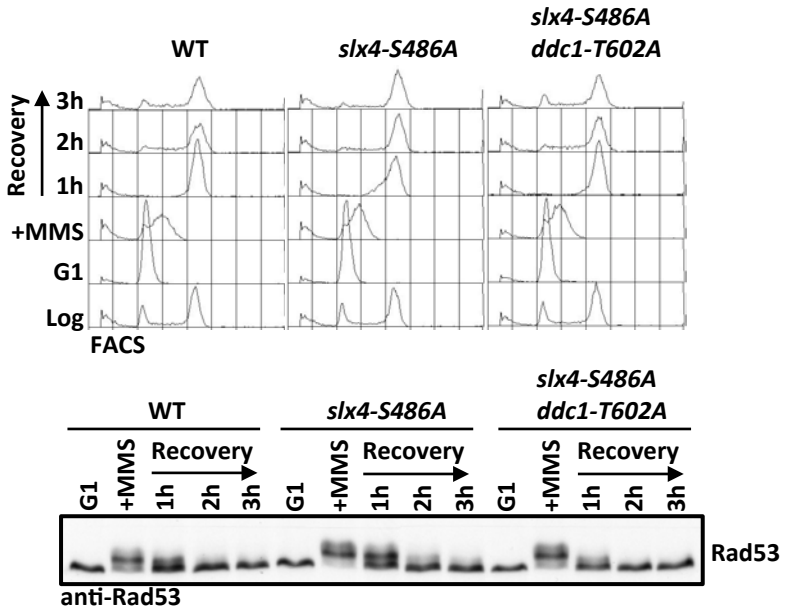
WT
slx4-S486A
slx4-S486A ddc1-T602A
Recovery
3h
2h
1h
+MMS
G1
Log
FACS
WT
slx4-S486A
slx4-S486A ddc1-T602A
G1
+MMS
Recovery
1h
2h
3h
Rad53
anti-Rad53

C

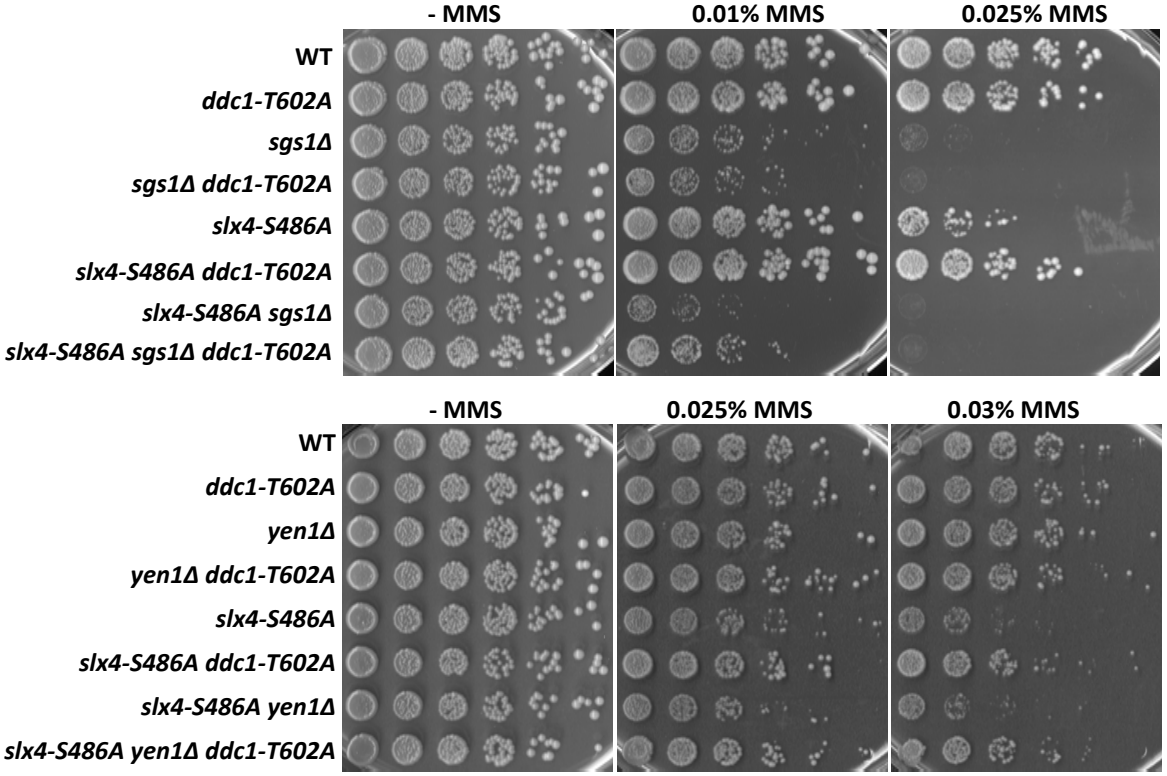
- MMS
0.01% MMS
0.025% MMS
WT
ddc1-T602A
sgs1Δ
sgs1Δ ddc1-T602A
slx4-S486A
slx4-S486A ddc1-T602A
slx4-S486A sgs1Δ
slx4-S486A sgs1Δ ddc1-T602A
- MMS
0.025% MMS
0.03% MMS
WT
ddc1-T602A
yen1Δ
yen1Δ ddc1-T602A
slx4-S486A
slx4-S486A ddc1-T602A
slx4-S486A yen1Δ
slx4-S486A yen1Δ ddc1-T602A

Supplemental Figure Legends

Figure S1.

The binding surface of the evolutionary conserved Slx4 and Dpb11 complex contains BRCT3+4 of Dpb11 and S486 of Slx4 in *S. cerevisiae*. **A** Slx4 binds to Dpb11 fragments containing BRCT3+4. Pulldown of Slx4 from undamaged or phleomycin-treated G1 or G2/M cell extracts using GST-Dpb11 fragments (N: aa 1-275, M: aa 276-600, C: aa 556-764, ΔC: aa 1-600). **B** Mutation of the Dpb11 BRCT3+4 phospho-protein binding surface reduces Slx4 binding to Dpb11. Two-hybrid analysis of GAL4-BD fused to *WT* Dpb11 or to Dpb11-T451A, and GAL4-AD fusions with Slx4. **C** A region in Slx4 sequence between aa 461 and aa 490 is important for Dpb11 interaction. Two-hybrid analysis of GAL4-BD (left panel) fused to *WT* Dpb11 or to the BRCT3+4 fragment, and GAL4-AD fusions with Slx4 C-terminal fragments. Expression of the constructs was verified by western blot analysis (right panel). **D** Mutation of S486 in Slx4 to a non-phosphorylatable alanine residue reduces Dpb11 binding. Two-hybrid analysis of GAL4-BD (left panel) fused to *WT* Dpb11 or to the BRCT3+4 fragment, and GAL4-AD fusions with *WT* Slx4 or with Slx4-S486A. Expression of the constructs was verified by western blot analysis (right panel). **E** The presence of DNA damage does not stimulate TopBP1 binding to Slx4 in human cells. Co-immunoprecipitation of ^{myc}TopBP1 with ^{GFP}Slx4 and ^{GFP}Slx4ΔN after transient overexpression in HEK 293T cells. Cells were left untreated or treated with 0.001% or 0.003% (++) MMS or 100 µg/ml zeocin for 30 min to induce DNA damage. **F** The Slx4-Dpb11 interaction is regulated by cell cycle phase and DNA damage. Co-

immunoprecipitation of Slx4 and Dpb11^{3FLAG} from G1 or G2/M arrested cells, which were either damaged by 50 µg/ml phleomycin or left untreated.

Figure S2.

A phosphorylation-dependent Dpb11/TopBP1 binding motif in eukaryotic Slx4 proteins.

Slx4 proteins from different eukaryotes comprise a conserved, short linear motif, which harbours serine 486 in budding yeast and threonine 1260 in humans. Multiple sequence alignment of the Dpb11/TopBP1 interaction motif. Conserved residues in more than one class are highlighted in yellow. Phosphorylation sites in *Saccharomyces cerevisiae* and *Homo sapiens*, as well as predicted sites as inferred from homology are indicated in red, alternative sites with unclear homology in light green. Species abbreviations, as well as accession numbers are listed in Supplementary Table 2.

Figure S3.

Mutation of seven SQ/TQ motifs in the C-terminus of Slx4 leads to similar phenotypes as the *slx4-S486A* mutation.

A The *slx4-S486A* and *slx4-7A* mutants are hyper-sensitive to MMS. *WT* or strains expressing *slx4-S486A* or the *slx4-7A* as only copy of Slx4 from the *SLX4* promoter were spotted in 5-fold serial dilutions on MMS-containing media and assayed for growth after two days. **B** Replication fork stalling is prolonged in the *slx4-S486A* and *slx4-7A* mutant. Cells were treated with a pulse of MMS during S-phase and recovery was analysed by pulsed-field gel electrophoresis to measure intact, fully replicated chromosomes. For

quantification, the fluorescence signal of chromosomes that migrated into the gel was divided by the total signal including the pocket and all signals normalized to the G1 sample from each strain. **C** The *Slx4-7A* and *Slx4-S486A* mutant proteins show reduced binding to Mms4 and Dpb11. Co-immunoprecipitation of endogenous Dpb11 and Slx4 with Mms4^{3FLAG} in combination with phosphorylation-deficient mutants of Slx4, S486A or 7A, or Slx4 deletion from G2/M arrested cells.

Figure S4.

Analysis of composition and function of the Slx4-Dpb11 complex.

A Slx4 and Dpb11 are part of a multi-protein complex containing Rtt107 and Slx1. Co-immunoprecipitations of Dpb11^{3FLAG} (left panel) and Slx4^{3FLAG} (right panel) were compared to purifications from untagged control strains using a SILAC setup. Cells were treated with 0.033% MMS, whereby strains containing Dpb11^{3FLAG}/Slx4^{3FLAG} were grown in heavy ($^{15}N_2$ $^{13}C_6$ lysine (Lys8) and $^{15}N_4$ $^{13}C_6$ arginine (Arg10)) medium, untagged control strains in light medium. Proteins shown in red are enriched in both purifications (Dpb11, Slx4, Rtt107, Slx1). The best scoring MS-MS spectra of the Slx4 peptide containing phosphorylated S486A from the Dpb11^{3FLAG} CoIP is shown. This peptide showed an H/L ratio of 17 in the Dpb11^{3FLAG} pulldown. **B** The *slx4-S486A* mutant is slightly sensitive to 4-NQO (in addition to MMS (Fig. 3B)), but not to other DNA damaging drugs. *WT* cells or the *slx4-S486A* mutant were spotted in 5-fold serial dilutions on media containing phleomycin, HU, CPT, cisplatin and 4-NQO and assayed for growth after two days. **C** The *slx4-S486A* mutant has a similar recombination rate compared to *WT*.

Recombination rates were measured using an intrachromosomal direct-repeat system (*leu2-112*::URA3::*leu2-k*, Aguilera and Klein 1988). Fluctuation analysis was performed using 10 independent cultures and recombinants were determined by plating on plates lacking leucine or leucine and uracil. Single colonies were counted and recombination rates were calculated using a maximum-likelihood method. The shown values represent means of three independent experiments. Error bars represent standard deviations. **D** The checkpoint response after treatment with DSB-inducing agents is similar in *WT* and *slx4-S486A* cells. Cells were treated with a 30 min pulse of 50 µg/ml phleomycin or zeocin during G2/M- or S-phase (see samples +Phl/+Zeo) and recovery was analysed by checkpoint activity as determined by anti-Rad53 western blot (upper panel) and by cellular DNA content as determined by FACS (lower panel).

Figure S5.

The Slx4-Dpb11 complex is not exclusively involved in either post-replicative repair (PRR) or homologous recombination (HR).

A A defect in the Dpb11-Slx4 complex further enhances the hyper-sensitivity of PRR and HR mutants. Strains expressing *slx4-S486A* as endogenous copy of Slx4 alone or in combination with mutants defective in error-free PRR (*mms2Δ*, *rad5-KT538,539AA* and *rad5-C914S*), error-prone PRR (*rev1Δ*, *rev3Δ* and *rad30Δ*) or HR (*rad51Δ*) were spotted in 5-fold serial dilutions on MMS-containing media and assayed for growth after two days. **B** The spontaneous mutagenesis rate of the *slx4-S486A* mutant is similar to *WT*. A forward mutagenesis assay was performed using a *CAN1* tester strain and

resistance to canavanine. Fluctuation analysis was carried out with 10 independent cultures. Colonies on canavanine-containing plates were counted and mutation rates were determined using a maximum-likelihood approach. The mean from 2 independent experiments is shown. Error bars represent standard deviations. **C** Up-regulation of HR at replication forks does not rescue the MMS hyper-sensitivity of *slx4-S486A* mutants. Strains expressing *WT* Slx4 or *slx4-S486A* in combination with *siz1Δ* or *srs2ΔC* were spotted as in A.

Figure S6.

The Slx4-Dpb11 complex is involved in JM resolution by Mus81-Mms4 and functions separately from Sgs1, Yen1 and Rad1-Rad10.

A DNA joint molecules form to a similar extent in *sgs1Δ* and *sgs1Δ slx4-S486A*. Cells were treated with 0.033% MMS in S-phase and after 90', 150' and 210' X-shaped JMs were visualized as spike signals in 2D gels. **B** JM structures are resolved slower in *slx4Δ tc-sgs1* cells. A conditional *sgs1* (*tc-sgs1)* allele was used because of *sgs1Δ slx4Δ* lethality (Mullen et al. 2001). In the *tc-sgs1* allele, Sgs1 translation is prevented upon addition of tetracycline (Gonzalez-Huici et al. 2014). *C*ells were treated with a pulse of MMS in S-phase and the profile of recombination intermediates was examined 0 h, 2 h, 3 h, 4 h and 6 h after release from MMS. X-shaped JMs were visualized as spike signal in 2D gels in *tc-sgs1* and *slx4Δ tc-sgs1* mutants. **C** The JM resolution defect in *slx4-S486A* mutants is weaker than in *mms4Δ* and both mutants show epistasis. *Tc-sgs1* inactivation and experiment as in B, but

samples were examined 0 h, 2 h, 3 h, 4 h and 5 h after release from MMS. **D** The Slx4-Dpb11 complex function in response to MMS is not related to the structure-specific endonucleases Rad1-Rad10, Slx1 or Yen1. Strains expressing *slx4-S486A* as endogenous copy of Slx4 alone or in combination with *rad1Δ, slx1Δ* and *yen1Δ* were spotted in 5-fold serial dilutions on MMS-containing media and assayed for growth after two days. **E** The *yen1Δ* increases MMS sensitivity of the *sgs1Δ slx4-S486A* double mutant, but not of either single mutant. *yen1Δ*, *sgs1Δ*, *slx4-S486A* mutants alone and double and triple mutant combinations were spotted as in D.

Figure S7.

Slx4 and Mus81 structures co-localize with Dpb11 anaphase bridge. A Quantification of Slx4 and Mus81 foci and bridges at Dpb11 anaphase bridges. *WT* or *sgs1*Δ cells expressing Dpb11^{CFP} and Slx4^{YFP}, Slx4-S486A^{YFP} or Mus81^{YFP} were subjected to live cell fluorescence microscopy. Representative examples of Slx4 and Mus81 foci and bridges co-localizing with Dpb11 anaphase bridges are shown. Scale bar, 3 μm. Yellow arrowhead marks foci. Error bars correspond to 95% confidence intervals. **B** Slx4^{YFP} and Mus81^{YFP} show a partial co-localization with Dpb11^{CFP} in spontaneous and DNA damage induced foci. Cells were treated with 0.03% MMS or 200 μg/ml zeocin for 1 h and co-localization (green arrow) of Dpb11^{CFP} with Slx4^{YFP} (top panel) and Mus81^{YFP} (lower panel) in foci was scored manually. Error bars correspond to 95% confidence intervals. Arrowheads mark foci.

Figure S8.

Mus81-Mms4 forms a complex with Dpb11 and Slx4.

A Mus81-Mms4 from mitotic cells binds specifically to Dpb11, Slx4 and Rtt107. A SILAC MS experiment comparing an Mms4^{3FLAG} IP to a control IP from an untagged strain using $^{15}N_2$ $^{13}C_6$ lysine (Lys8) and Lys-C digestion is shown. All cells were arrested in mitosis by nocodazole. H/L ratios from two label-switch experiments without ratio count cut-off are plotted. #, as the only protein of the analysis Dpb11 displayed exclusively peptides, which were derived from the Mms4^{3FLAG} IP samples, but not the control samples, making Dpb11 a highly specific interactor of Mus81-Mms4. **B** Slx4, Dpb11 and Mus81-Mms4 are part of one multi-protein complex. Mms4^{3FLAG} immunoprecipitates (as in A) from G2/M arrested cells were subjected to glycerol gradient (10%-30%) centrifugation. Slx4, Dpb11 and Mms4 co-migrate in fractions 18-20 (marked by box), corresponding to a multi-protein complex with an apparent molecular weight of 1-1.5 MDa. Arrowheads indicate elution peaks of single proteins. **C** The Dpb11-Mms4 interaction is independent of Slx4. Two-hybrid analysis in WT and *slx4Δ* cells with Gal4-BD-Dpb11 and Gal4-AD-Mms4. **D** Dpb11 and Slx4 binding to Mms4 is partially phosphatase-sensitive. Mms4^{3FLAG} immunoprecipitates (as in A) from G2/M arrested cells were either mock treated or treated with 24,000 U/ml λ-phosphatase for 20 min at 4°C. Shown is the phosphatase eluate and a 3xFLAG peptide-eluate of the remaining bound material.

Figure S9.

Mus81-Mms4 show a Cdc5-dependent association with Slx4-Dpb11 in mitosis. A Mms4 interaction with the Slx4-Dpb11 complex is dependent on Polo-like kinase Cdc5 activity. *CDC5* was expressed from a pGAL1-10 promoter. Cells were grown in raffinose-containing medium, arrested in G1, then expression was either induced in G1 by switching cells to galactose-containing medium prior to G2/M arrest (lane 2) or shut-off in G1 by switching cells to glucose-containing medium (lane 3). Co-immunoprecipitations of Mms4^{3FLAG} were performed from the corresponding cell extracts and tested for binding to Dpb11 and Slx4. **B** CDK activity is not influenced by interfering with Cdc5 activity. TCA samples of experiments shown in Fig. 5C and Fig. S9A were tested for CDK-mediated phosphorylation of Rad9-T474 by using a phospho-specific antibody in western blot analysis. The asterisk denotes a cross-reactive band. **C** The Slx4-Dpb11 interaction is not dependent on the Polo-like kinase Cdc5. Co-immunoprecipitation of Dpb11 and Slx4^{3FLAG} from G2/M arrested cells or G2/M arrested cells, in which Cdc5 has been inactivated by using the *cdc5-as1* allele and 10 µM CMK. **D** The formation of the Slx4-Dpb11-Mms4-Mus81 complex is not influenced by the presence of DNA damage. Co-immunoprecipitation samples of Mms4^{3FLAG} cell extracts from G2/M arrested cells, which were either damaged by 50 µg/ml phleomycin or left untreated, were tested for binding to Dpb11 and Slx4. **E** Cell cycle regulation of Mus81-Mms4 nuclease activity remains intact in the *slx4-S486A* mutant. Mms4^{3FLAG} and control IPs from cells arrested at G2/M with nocodazole (see lower panel for the inputs) were incubated with

fluorescence-labelled Holliday junction, replication fork and nicked Holliday junction substrates.

Figure S10.

Partial inactivation of the DNA damage checkpoint rescues the defects of the *slx4-S486A* mutant in response to MMS.

A A partial defect in DNA damage checkpoint signalling suppresses the *slx4-S486A* mutant hyper-sensitivity to MMS. Strains expressing *slx4-S486A* in combination with mutants defective in DNA damage checkpoint signalling (*dot1Δ, ddc1-T602A* and *rad53-3HA)* were spotted in 5-fold serial dilutions on MMS-containing media and assayed for growth after two days. **B** The *slx4-S486A* mutant recovers faster after a partial inactivation of the DNA damage checkpoint. *WT*, *slx4-S486A* and *slx4-S486A ddc1-T602A* mutant cells were treated with a pulse of 0.033% MMS during S-phase, and recovery was analysed by cellular DNA content as determined by FACS (upper panel) and by checkpoint activity as determined by anti-Rad53 western blot (lower panel). **C** Yen1 and Sgs1 are not required for the rescue of the *slx4-S486A* MMS hyper-sensitivity by partial checkpoint inactivation. MMS hyper-sensitivity phenotypes of *slx4-S486A*, *sgs1Δ*, *yen1Δ*, *ddc1-T602A* mutants and double or triple mutant combinations were spotted in 5-fold serial dilutions on MMS-containing media and assayed for growth after two (lower panel) or three (upper panel) days.

Supplemental Methods

Yeast strains

All yeast strains are based on W303 (Thomas and Rothstein 1989). Genotypes are listed below. All biochemical experiments were performed in a W303-1A *pep4Δ* background. The genetic studies in Fig. 3B-E, 4, 6A-E and Fig. S3A-B, S4B-D, S5, S6, S10 were performed in a W303 *RAD5+* background to exclude any effect from a partial defect of the *rad5-535* allele, but similar results were obtained using W303-1A. Two-hybrid analyses were performed in the strain PJ69-7A (James et al. 1996).

S. cerevisiae strains were prepared by genetic crosses and transformation techniques. Deletion of particular genes and endogenous protein tagging were performed as described (Knop et al. 1999). Correct integrations were checked by genotyping PCR. Denaturing cell extracts were prepared by alkaline lysis and TCA precipitation (Knop et al. 1999). The *slx4-S486A* allele was generated using site-directed mutagenesis and integrated as a linear plasmid at the TRP1 locus.

List of strains used in this study.

Strain	Full genotype	Relevant genotype	Source
1093-5A	MATa *ADE2+ RAD5+ CAN1+ ura3-1 his3-11,15 trp1-1 leu2-3,112*	*CAN1+*	Klein lab
FY1060	MATa *RAD5+ ade2-1 ura3-1 his3-11,15 trp1-1 leu2-3,112 can1-100 GAL PSI+ sgs1::HIS3*	*sgs1*	Branzei lab
HY4021	MATa *RAD5+ ade2-1 trp1-1 leu2-3,112 his3-11,15 ura3-1 can1-100 sgs1::pADH1-tc3-3xHA-Sgs1*	*Tc-SGS1*	Branzei lab

	(NATMX)		
HY4072	MATa *RAD5+ ade2-1 trp1-1 leu2-3,112 his3-11,15 ura3-1 can1-100 slx4::HIS3 sgs1::pADH1-tc3-3xHA-Sgs1 (HPHMX4)*	*slx4 Tc-SGS1*	Branzei lab
ML664-10A	MATa *tTA(tetR-VP16)-tetO$_2$-DPB11-4ala-YFP*::*KanMX NLS-yEmRFPrv::URA3 SPC110-CFP::KAN*	*DPB11-YFP SPC110-CFP*	Lisby lab
ML678-12B	MATa *tTA(tetR-VP16)-tetO$_2$-DPB11-4ala-YFP*::*KanMX NLS-yEmRFPrv::URA3 SPC110-CFP::KanMX sgs1::HIS3*	*DPB11-YFP SPC110-CFP sgs1*	Lisby lab
ML779-4A	MATa *tTA(tetR-VP16)-tetO$_2$-DPB11-4ala-YFP*::*KanMX NLS-yEmRFPrv::URA3 SPC110-CFP::KanMX slx4::KanMX*	*DPB11-YFP SPC110-CFP slx4*	Lisby lab
ML781-8D	MATa *tTA(tetR-VP16)-tetO$_2$-DPB11-4ala-YFP*::*KanMX NLS-yEmRFPrv::URA3 SPC110-CFP::KanMX slx4::KanMX trp1-1::slx4-S486A::TRP1*	*DPB11-YFP SPC110-CFP slx4 slx4-S486A*	Lisby lab
ML798-4C	MATa *tTA(tetR-VP16)-tetO$_2$-DPB11-4ala-YFP*::*KanMX NLS-yEmRFPrv::URA3 SPC110-CFP::KanMX slx4::KanMX trp1-1::slx4-S486A::TRP1 sgs1::HIS3*	*DPB11-YFP SPC110-CFP slx4 slx4-S486A sgs1*	Lisby lab
ML789-7D	MATa *ade2-1 ura3-1 his3-11,15 trp1-1 leu2-3,112 can1-100 tTA(tetR-VP16)-tetO$_2$-DPB11-4ala-CFP::KanMX SLX4-4ala-YFP*	*DPB11-CFP SLX4-YFP*	Lisby lab
ML799-2C	MATa *tTA(tetR-VP16)-tetO$_2$-DPB11-4ala-CFP*::*KanMX SLX4-YFP sgs1::HIS3*	*DPB11-CFP SLX4-YFP sgs1*	Lisby lab
ML806-3C	MATa *tTA(tetR-VP16)-tetO$_2$-DPB11-4ala-CFP*::*KanMX slx4-S486A-YFP*	*DPB11-CFP slx4-S486A-YFP*	Lisby lab
ML806-3A	MATa *tTA(tetR-VP16)-tetO$_2$-DPB11-4ala-CFP*::*KanMX slx4-S486A-YFP sgs1::HIS3*	*DPB11-CFP slx4-S486A-YFP sgs1*	Lisby lab
ML792-2D	MATa *ade2-1 ura3-1 his3-11,15 trp1-1 leu2-3,112 can1-100*	*DPB11-CFP MUS81-YFP*	Lisby lab

	tTA(tetR-VP16)-tetO$_2$-DPB11-4ala-CFP::KanMX MUS81-4ala-YFP		
ML800-9A	MATa *tTA(tetR-VP16)-tetO$_2$-DPB11-4ala-CFP*::*KanMX MUS81-YFP sgs1::HIS3*	*DPB11-CFP MUS81-YFP sgs1*	Lisby lab
Y2050	MATα *ade2-1 trp1-1 his3-11 his3-15 can1-100 leu2-112::URA3::leu2-k*	*leu2-112::URA3::leu2-k*	Jentsch lab
YBP388	MATa *ade2-1 ura3-1 his3-11,15 leu2-3,112 can1-100 leu2-3,112::pep4::LEU2*	*pep4*	This study
YBP392	MATa *ade2-1 ura3-1 his3-11,15 leu2-3,112 can1-100 trp1-1::bar1::TRP1 leu2-3,112::pep4::LEU2*	*bar1 pep4*	This study
YBP418-1	MATa *ade2-1 ura3-1 his3-11,15 can1-100 lys1::NAT-NT2 arg4::hph-NT1 trp1-1::bar1::TRP1 leu2-3,112::pep4::LEU2 SLX4-3FLAG::KanMx4*	*lys1 SLX4-3FLAG*	This study
YBP420	MATa *ade2-1 ura3-1 his3-11,15 can1-100 arg4::hph-NT2 lys1::NAT-NT1 leu2-3,112::pep4::LEU2 trp1-1::bar1::TRP1*	*lys1 arg4*	This study
YBP422	MATa *ade2-1 ura3-1 his3-11,15 can1-100 arg4::hph-NT2 lys1::NAT-NT1 leu2-3,112::pep4::LEU2 trp1-1::bar1::TRP1 DPB11-3FLAG::KanMx*	*lys1 arg4 DPB11-3FLAG*	This study
YDG40	MATα *ade2-1 ura3-1 his3-11,15 leu2-3,112 can1-100 slx4::kanMx4 trp1-1::slx4-S486A::TRP1*	*slx4-S486A*	This study
YDG66	MATa *ade2-1 ura3-1 his3-11,15 trp1-1 leu2-3,112 can1-100 rad51::natNT2*	*rad51*	This study
YDG96	MATα *ade2-1 trp1-1 his3-11 his3-15 can1-100 leu2-112::URA3::leu2-k slx4::kanMx slx4-S486A::TRP1*	*leu2-112::URA3::leu2-k slx4-S486A*	This study

YDG126	MATa *ade2-1 ura3-1 his3-11,15 trp1-1 leu2-3,112 can1-100 rad1::hphNTI*	*rad1*	This study
YDG134	MATa *ade2-1 ura3-1 his3-11,15 trp1-1 leu2-3,112 can1-100 slx1::hphNTI*	*slx1*	This study
YDG135	MATa *ade2-1 ura3-1 his3-11,15 leu2-3,112 can1-100 slx4::KanMx trp1-1::slx4-S486A::TRP1 slx1::hphNTI*	*slx4-S486A slx1*	This study
YDG150	MATa *ade2-1 ura3-1 his3-11,15 trp1-1 leu2-3,112 can1-100 mms2::hphNTI*	*mms2*	This study
YDG151	MATα *ade2-1 ura3-1 his3-11,15 leu2-3,112 can1-100 slx4::kanMx trp1-1::slx4-S486A::TRP1 mms2::hphNTI*	*slx4-S486A mms2*	This study
YDG175	MATa *ade2-1 ura3-1 his3-11,15 trp1-1 leu2-3,112 can1-100 rad5::hphNTI*	*rad5*	This study
YDG182	MATa *ade2-1 ura3-1 his3-11,15 leu2-3,112 can1-100 slx4::kanMx trp1-1::slx4-S486A::TRP1 rad51::hphNT1*	*slx4-S486A rad51*	This study
YDG183	MATa *ade2-1 ura3-1 his3-11,15 trp1-1 leu2-3,112 can1-100 rev1::hphNT1*	*rev1*	This study
YDG184	MATa *ade2-1 ura3-1 his3-11,15 leu2-3,112 can1-100 slx4::kanMx trp1-1::slx4-S486A::TRP1 rev1::hphNT1*	*slx4-S486A rev1*	This study
YDG185	MATa *ade2-1 ura3-1 his3-11,15 trp1-1 leu2-3,112 can1-100 rev3::hphNT1*	*rev3*	This study
YDG186	MATa *ade2-1 ura3-1 his3-11,15 leu2-3,112 can1-100 slx4::kanMx trp1-1::slx4-S486A::TRP1 rev3::hphNT1*	*slx4-S486A rev3*	This study
YDG187	MATa *ade2-1 ura3-1 his3-11,15 trp1-1 leu2-3,112 can1-100 rad30::hphNT1*	*rad30*	This study
YDG188	MATa *ade2-1 ura3-1 his3-11,15 leu2-3,112 can1-100 slx4::kanMx*	*slx4-S486A rad30*	This study

	trp1-1::slx4-S486A::TRP1 rad30Δ::hphNT1		
YDG189	MATa *RAD5+ ade2-1 ura3-1 leu2-3,112 can1-100 slx4::kanMx trp1-1::slx4-S486A::TRP1 his3-11,15::sgs1::HIS3*	*slx4-S486A sgs1*	This study
YDG190	MATa *RAD5+ ade2-1 ura3-1 his3-11,15 leu2-3,112 can1-100 slx4::kanMx trp1-1::slx4-S486A::TRP1*	*slx4-S486A*	This study
YDG206	MATα *RAD5+ CAN1+ ADE2+ ura3-1 his3-11,15 leu2-3,112 slx4::kanMx4 trp1-1::slx4-S486A::TRP1*	*CAN1+ slx4-S486A*	This study
YDG207	MATa *CAN1+* ADE2+ *ura3-1 his3-11,15 trp1-1 leu2-3,112 rad5::hphNT1*	*CAN1+ rad5*	This study
YDG209	MATa *ade2-1 his3-11,15 trp1-1 leu2-3,112 can1-100 rad5::hphNT1 ura3-1::RAD5+::URA3*	*rad5 RAD5+*	This study
YDG211	MATa *ade2-1 his3-11,15 trp1-1 leu2-3,112 can1-100 rad5::hphNT1 ura3-1::rad5+-C914S::URA3*	*rad5+-C914S*	This study
YDG212	MATa *ade2-1 his3-11,15 leu2-3,112 can1-100 slx4::kanMx4 trp1-1::slx4-S486A::TRP1 rad5::hphNT1 ura3-1::RAD5+::URA3*	*slx4-S486A rad5Δ RAD5+*	This study
YDG214	MATa *ade2-1 his3-11,15 leu2-3,112 can1-100 slx4::kanMx4 trp1-1::slx4-S486A::TRP1 rad5::hphNT1 ura3-1::rad5+-C914S::URA3*	*slx4-S486A rad5+-C914S*	This study
YDG217	MATa *RAD5+ ade2-1 his3-11,15 trp1-1 ura3-1 leu2-3,112 can1-100 srs2ΔC::hphNT1*	*srs2ΔC*	This study
YDG218	MATa *RAD5+ ade2-1 his3-11,15 ura3-1 leu2-3,112 can1-100 slx4::kanMx4 trp1-1::slx4-S486A::TRP1 srs2ΔC::hphNT1*	*slx4-S486A srs2ΔC*	This study
YDG219	MATa *RAD5+ ade2-1 his3-11,15*	*siz1*	This

	trp1-1 ura3-1 leu2-3,112 can1-100 siz1::hphNT1		study
YDG220	MATa *Rad5+ ade2-1 his3-11,15 ura3-1 leu2-3,112 can1-100 slx4::kanMx4 trp1-1::slx4-S486A::TRP1 siz1::hphNT1*	*slx4-S486A siz1*	This study
YDG240	MATa *ade2-1 his3-11,15 trp1-1 leu2-3,112 can1-100 rad5::hphNT1 ura3-1::rad5+-KT538,539AA::URA3*	*rad5+-KT538,539AA*	This study
YDG241	MATa *ade2-1 his3-11,15 leu2-3,112 can1-100 rad5::hphNT1 ura3-1:rad5+-KT538,539AA::URA3 slx4::kanMx4 trp1-1::slx4-S486A::TRP1*	*slx4-S486A rad5+-KT538,539AA*	This study
YDG251	MATa *RAD5+ ade2-1 leu2-3,112 ura3-1 trp1-1 can1-100 his3-11,15::rad53-3HA::HIS3*	*rad53-3HA*	This study
YDG252	MATa *RAD5+ ade2-1 leu2-3,112 ura3-1 can1-100 slx4Δ::kanMx4 trp1-1::slx4-S486A::TRP1 his3-11,15::rad53-3HA::HIS3*	*slx4-S486A rad53-3HA*	This study
YDG287	MATa *RAD5+ ade2-1 his3-11,15 leu2-3,112 ura3-1 can1-100 slx4::kanMx4 trp1-1::slx4-S486A::TRP1 dot1::natNT2*	*slx4-S486A dot1*	This study
YDG288	MATa *RAD5+ ade2-1 his3-11,15 leu2-3,112 ura3-1 can1-100 slx4::kanMx4 trp1-1::slx4-S486A::TRP1 ddc1-T602A::natNT2*	*slx4-S486A ddc1-T602A*	This study
YDG289	MATa *RAD5+ ade2-1 his3-11,15 leu2-3,112 trp1-1 ura3-1 can1-100 mms4::hphNT1*	*mms4*	This study
YDG290	MATa *RAD5+ ade2-1 his3-11,15 leu2-3,112 ura3-1 can1-100 slx4::kanMx4 trp1-1::slx4-S486A::TRP1 mms4::hphNT1*	*slx4-S486A mms4*	This study
YDG291	MATa *RAD5+ ade2-1 his3-11,15 leu2-3,112 trp1-1 ura3-1 can1-100 yen1::hphNT1*	*yen1*	This study
YDG292	MATa *RAD5+ ade2-1 his3-11,15*	*slx4-S486A yen1*	This

	leu2-3,112 ura3-1 can1-100 slx4::kanMx4 trp1-1::slx4-S486A::TRP1 yen1::hphNT1		study
YDG293	MATa *RAD5+ ade2-1 his3-11,15 leu2-3,112 ura3-1 can1-100 slx4::kanMx trp1-1::DPB11-slx4-S486A::TRP1*	*DPB11-slx4-S486A*	This study
YDG295	MATa *RAD5+ ade2-1 his3-11,15 leu2-3,112 ura3-1 can1-100 slx4::kanMx4 trp1-1::slx4-S486A::TRP1 ddc1-T602A::natNT2 yen1::hphNT1*	*slx4-S486A ddc1-T602A yen1*	This study
YDG296	MATa *RAD5+ ade2-1 his3-11,15 leu2-3,112 trp1-1 ura3-1 can1-100 ddc1-T602A::natNT2 yen1::hphNT1*	*ddc1-T602A yen1*	This study
YDG329	MATa *RAD5+ ade2-1 ura3-1 his3-11,15 trp1-1 leu2-3,112 can1-100 sgs1::hphNT1*	*sgs1*	This study
YDG303	MATa *Rad5+ ade2-1 his3-11,15 leu2-3,112 trp1-1 ura3-1 can1-100 ddc1-T602A::natNT2*	*ddc1-T602A*	This study
YDG304	MATa *RAD5+ ade2-1 his3-11,15 leu2-3,112 trp1-1 ura3-1 can1-100 dot1::natNT2*	*dot1*	This study
YDG309	MATa *RAD5+ ade2-1 his3-11,15 leu2-3,112 ura3-1 can1-100 slx4::kanMx4 trp1-1::slx4-S486A::TRP1 ddc1-T602A::natNT2 mms4::hphNT1*	*slx4-S486A ddc1-T602A mms4*	This study
YDG310	MATa *RAD5+ ade2-1 his3-11,15 leu2-3,112 trp1-1 ura3-1 can1-100 ddc1-T602A::natNT2 mms4::hphNT1*	*ddc1-T602A mms4*	This study
YDG313	MATa *RAD5+ ade2-1 his3-11,15 leu2-3,112 ura3-1 can1-100 slx4::kanMx4 trp1-1::slx4-S486A::TRP1 ddc1-T602A::natNT2 sgs1::hphNT1*	*slx4-S486A ddc1-T602A sgs1*	This study
YDG314	MATa *RAD5+ ade2-1 his3-11,15 leu2-3,112 trp1-1 ura3-1 can1-100 ddc1-T602A::natNT2 sgs1::hphNT1*	*ddc1-T602A sgs1*	This study

YDG335	MATa *RAD5+ ade2-1 ura3-1 his3-11,15 leu2-3,112 trp1-1 can1-100 mus81Δ::hphNT1*	*mus81*	This study
YDG336	MATa *RAD5+ ade2-1 ura3-1 his3-11,15 leu2-3,112 can1-100 slx4::kanMx4 trp1-1::slx4-S486A::TRP1 mus81::hphNT1*	*slx4-S486A mus81*	This study
YDG339	MATa *RAD5+ ade2-1 ura3-1 his3-11,15 trp1-1 leu2-3,112 can1-100 MMS4-3FLAG::hphNTI*	*MMS4-3FLAG*	This study
YDG340	MATa *RAD5+ ade2-1 ura3-1 his3-11,15 leu2-3,112 can1-100 slx4::kanMx trp1-1::slx4-S486A::TRP1 MMS4-3FLAG::hphNTI*	*slx4-S486A MMS4-3FLAG*	This study
YDG355	MATa *RAD5+ ade2-1 his3-11, 15 trp1-1 ura3-1 can1-100 mms4::hphNTI leu2-3,112::mms4SS184,201AA::LEU2*	*mms4-SS184,201AA*	This study
YDG356	MATa *RAD5+ ade2-1 trp1-1 ura3-1 can1-100 mms4::hphNTI leu2-3,112::mms4SS184,201AA::LEU2 his3-11,15::sgs1::HIS3*	*mms4-SS184,201AA sgs1*	This study
YDG366	MATa *RAD5+ ade2-1 his3-1,15 leu2-3,112 ura3-1 can1-100 slx4::kanMx trp1-1::slx4-S486A::TRP1 ddc1-T602A::natNT2 MMS4-3FLAG::hphNTI*	*slx4-S486A ddc1-T602A MMS4-3FLAG*	This study
YDG375	MATa *RAD5+ ade2-1 ura3-1 his3-11,15 leu2-3,112 can1-100 slx4::NAT trp1-1::slx4-7A::TRP1*	*slx4-T457A, T474A, S499A, T597A, S627A, S659A, S725A*	This study
YDG376	MATa *RAD5+ ade2-1 ura3-1 his3-11,15 trp1-1 leu2-3,112 can1-100 yen1::hphNT1 sgs1::natNT2*	*yen1 sgs1*	This study
YDG377	MATa *RAD5+ ade2-1 ura3-1 his3-11,15 leu2-3,112 can1-100 slx4::kanMx trp1-1::slx4-S486A::TRP1 yen1Δ::hphNT1 sgs1::natNT2*	*slx4-S486A yen1 sgs1*	This study

YKR44	MATa *ade2-1 ura3-1 his3-11 his3-15 can1-100 trp1-1::bar1::TRP1 leu2-3,112::pep4::LEU2 DPB11-9myc::KanMX4*	*DPB11-9myc*	This study
YLP15	MATa *ade2-1 ura3-1 his3-11 his3-15 can1-100 trp1-1::bar1::TRP1 leu2-3,112::pep4::LEU2 lys1::nat-NT2*	*lys1*	This study
YLP18	MATa *ade2-1 ura3-1 can1-100 trp1-1::bar1::TRP1 leu2-3,112::pep4::LEU2 lys1::nat-NT2 his3-11,15::SLX4-3FLAG::HisMx*	*lys1 SLX4-3FLAG*	This study
YLP30	MATa *ade2-1 ura3-1 trp1-1 leu2-3,112 can1-100 pep4::NAT slx4::KanMx his3-11,15::slx4-S486A-3FLAG::HISMx*	*slx4-S486A-3FLAG*	This study
YLP41	MATa *ade2-1 ura3-1 trp1-1 leu2-3,112 can1-100 his3-11,15::slx4-S486A-3FLAG::HisMx pep4::NAT lys1::hph*	*lys1 slx4-S486A-3FLAG*	This study
YLP42	MATa *ade2-1 his3-11 his3-15 can1-100 trp1-1::bar1::TRP1 leu2-3,112::pep4::LEU2 SLX4-3FLAG::KanMx4 ura3-1::cdc28as-1 F88G::URA3*	*SLX4-3FLAG cdc28-as1*	This study
YLP43	MATa *ade2-1 his3-11,15 can1-100 lys1::hph trp1-1::bar1::TRP1 leu2-3,112::pep4::LEU2 SLX4-3FLAG::KanMx4 ura3-1::cdc28as-1 F88G::URA*	*lys1 SLX4-3FLAG cdc28-as1*	This study
YLP47	MATa *ade2-1 ura3-1 can1-100 trp1-1::bar1::TRP1 leu2-3,112::pep4::LEU2 his3-11,15::DPB11-3Flag::HIS3*	*DPB11-3FLAG*	This study
YLP57	MATa *RAD5+ ade2-1 ura3-1 trp1-1 leu2-3,112 can1-100 MMS4-3Flag::hphNTI his3-11,15::pep4::HIS3*	*MMS4-3FLAG*	This study
YLP59	MATa *ade2-1 ura3-1 trp1-1 leu2-3,112 can1-100 MMS4-3Flag::hph-NT1 his3-11,15::pep4::HIS3Mx4 pGAL1-*	*MMS4-3FLAG pGal1-Cdc5*	This study

	CDC5::KanMx		
YLP62	MATa *ade2-1 ura3-1 leu2-3,112 can1-100 MMS4-3Flag::hph-NT1 his3-11,15::pep4::HIS3Mx4 slx4::KanMx trp1-1::slx4-S486A::TRP1*	*MMS4-3FLAG slx4-S486A*	This study
YLP63	MATa *RAD5+ ade2-1 ura3-1 trp1-1 leu2-3,112 can1-100 cdc5-as1 MMS4-3Flag::hph-NT1 his3-11,15::pep4::HIS3Mx4*	*MMS4-3FLAG cdc5-as1*	This study
YLP64	MATa *RAD5+ ade2-1 leu2-3,112 ura3-1 can1-100 slx4::kanMx trp1-1::slx4-S486A::TRP1 ddc1T602A:: natNT2 MMS4-3Flag::hphNTI his3-11,15::pep4::HIS3Mx4*	*MMS4-3FLAG slx4-S486A ddc1-T602A*	This study
YLP78	MATa *ade2-1 leu2-3,112 trp1-1 ura3-1 can1-100 MMS4-3Flag::hph-NT1 his3-11,15::pep4::HIS3Mx4 slx4::KanMx*	*MMS4-3FLAG slx4*	This study
YLP80	MATa *RAD5+ ade2-1 leu2-3,112 ura3-1 can1-100 MMS4-3Flag::hph-NT1 his3-11,15::pep4::HIS3Mx4 slx4::KanMx trp1-1::Slx4 T457A, T474A, S499A, T597A, S627A, S659A, S725A::TRP1*	*MMS4-3FLAG slx4-T457A, T474A, S499A, T597A, S627A, S659A, S725A*	This study
YLP83	MATa *RAD5+ ade2-1 his3-1,15 trp1-1 ura3-1 can1-100 leu2-3,112::pep4::LEU2 SLX4-3Flag::KanMx4 cdc5-as1*	*SLX4-3FLAG cdc5-as1*	This study
YLP87	MATa *RAD5+ ade2-1 leu2-3,112 trp1-1 ura3-1 can1-100 his3-11,15::pep4::HIS*	*pep4*	This study
YLP88	MATa *RAD5+ ade2-1 leu2-3,112 ura3-1 can1-100 slx4Δ::kanMx trp1-1::slx4-S486A::TRP1 MMS4-3Flag::hphNTI his3-11,15::pep4::HIS*	*MMS4-3FLAG slx4-S486A*	This study
YSB79	MATa *RAD5+ ade2-1 ura3-1 his3-11,15 leu2-3,112 trp1-1 can1-100 RFA1-*	*RFA1-3xmCherry*	This study

	3xmCherry::hphNT1		
YSB86	MATa *RAD5+ ade2-1 ura3-1 his3-11,15 leu2-3,112 trp1-1 can1-100 RFA1-3xmCherry::hphNT1 slx4::kanMx4 trp1-1:Slx4-S486A::TRP1*	*RFA1-3xmCherry slx4-S486A*	This study
YSS3	MATa *ade2-1 ura3-1 trp1-1 leu2-3,112 can1-100 MMS4-3Flag::hph-NT1 his3-11,15::pep4::HIS3Mx4*	*MMS4-3FLAG*	This study
YSS5	MATa *ade2-1 ura3-1 his3-11,15 can1-100 trp1-1::bar1::TRP1 leu2-3,112::pep4::LEU2 SLX4-3Flag::KanMx4*	*SLX4-3FLAG*	This study

Synchronization by α-factor and nocodazole

Logarithmic growing cells were synchronized in G2/M-phase by nocodazole (5 μg/ml), or in G1-phase by α-factor (5-10 μg/ml, or 167 ng/ml for *bar1* cells). The release from synchronization was performed by washing once in YPD, and suspending cells in YPD with 0.033% or 0.04% MMS. For recovery experiments, cells were washed after 30' (45' in Fig. 6E, S3B) of damage treatment, and suspended in drug free YPD media with (Fig. 5D, 6E-F) or without nocodazole.

Drug treatment

DNA damage in liquid cultures was induced by MMS (final concentration 0.033%, or 0.04% (Fig. 3C-E, 6D)) or phleomycin/zeocin (final concentration 50 μg/ml).

For solid media, concentrations of methyl methanesulfonate (MMS), hydroxyurea (HU), phleomycin, cisplatin, camptothecin (CPT) or 4-nitroquinoline 1-oxide (4-NQO) were as indicated in the figures.

FACS analysis

$1x10^7$ - $2x10^7$ cells were harvested by centrifugation and resuspended in 70% ethanol + 50 mM Tris pH 7.8. After centrifugation cells were washed with 1 ml 50 mM Tris pH 7.8 (Tris buffer) followed by resuspending in 520 µl RNase solution (500 µl 50 mM Tris pH 7.8 + 20 µl RNase A (10 mg/ml in 10 mM Tris pH 7.5, 10 mM $MgCl_2$) and incubation for 4 h at 37 °C. Next, cells were treated with proteinase K (200 µl Tris buffer + 20 µl proteinase K (10 mg/ml in 50% glycerol, 10 mM Tris pH 7.5, 25 mM $CaCl_2$) and incubated for 30' at 50 °C. After centrifugation cells were resuspended in 500 µl Tris buffer. Before measuring the DNA content, samples were sonified (5''; 50% CYCLE) and stained by SYTOX solution (999 µl Tris buffer + 1 µl SYTOX). Measurement was performed using FL1 channel 520 for SYTOX-DNA on a BD FACSCalibur system.

Interaction assays

After cell growth under the indicated conditions, yeast extracts were obtained by freezer mill lysis in lysis buffer (100 mM Hepes, 200 mM KOAc, 0.1 % NP-40, 10 % glycerol, 2 mM b-ME, protease inhibitors, 100 mM ocadaic acid, 10 mM NaF, 20 mM b-glycerophosphate). Co-IP was performed for 2 hours by head-over-tail rotation at 4 °C using anti-FLAG agarose resin (Sigma). Non-specific background was removed by six washes and bound proteins were

eluted by incubation with 0.5 mg/ml 3X FLAG-peptide (Sigma). The TCA precipitated eluates were resolved on 4-12% NuPAGE gradient gels (Invitrogen), and analyzed by standard Western blotting techniques.
For GST pulldowns (Fig. S1A), GST-Dpb11 or GST-tagged protein fragments were recombinantly expressed and purified as described (Pfander and Diffley 2011). Proteins were immobilizied on glutathione sepharose 4B (GE Healthcare) and incubated with ammonium sulphate-precipitated (57%) yeast extracts (lysis buffer as described above). Non-specific background was removed by five washes and bound proteins were eluted by Laemmli buffer.
For Co-IP from HEK 293T cells were lysed in lysis buffer (see yeast lysates) for 30' on ice. Protein concentrations were determined by Bradford. GFP-tagged proteins were precipitated using GFP-Trap magnetic beads (Chromotek) and incubated for 1.5 h with head-over-tail rotation. Non-specifically bound proteins were removed by 6 washes with lysis buffer using a magnetic rack, and specifically bound proteins were eluted by Laemmli buffer.

Analysis of interacting proteins by SILAC

For Co-IP experiments followed by mass spectrometry analysis, cells deficient in lysine biosynthesis were grown in synthetic complete (SC) medium supplemented with normal lysine ("light" medium) or heavy-isotope-labeled lysine (Lys8; "heavy" medium) from Cambridge Isotope Laboratories.
For SILAC Co-IP experiments shown in Fig. S4A, cells deficient in lysine and arginine biosynthesis were grown in synthetic complete (SC) medium supplemented with normal lysine and arginine ("light" medium) or heavy-

isotope-labeled lysine and arginine (Lys8, Arg10; “heavy” medium) from Cambridge Isotope Laboratories. All other SILAC experiments were done using lysine-only labeling.

Lysates were prepared by harvesting cells in equal amounts after growth under the indicated conditions. After co-IP, eluted proteins from light and heavy cultures were pooled, TCA precipitated and separated on 4-12% NuPAGE Bis-Tris gel (Invitrogen). The gel was stained with GelCode Blue (Thermo Scientific). The gel lane was excided into ten slices and peptides were analyzed by LC-MS/MS after in-gel Lys-C or trypsin digestion. Samples were measured on an LTQ-Orbitrap and analyzed using MaxQuant (Cox and Mann 2008).

Antibodies

Proteins were detected using specific antibodies: rabbit-anti-Rad53 (JD147, J. Diffley), rabbit-anti-Dpb11 (BPF19; Pfander and Diffley 2011), rabbit-anti-Rad9-T474-P (BPF25, Pfander and Diffley 2011), rabbit-anti-Slx4 (2057, Pfander lab), goat-anti-Cdc5 (sc-6733, Santa Cruz), rabbit-anti-Clb2 (sc-9071, Santa Cruz), rabbit-anti-FLAG (Sigma), rabbit-HRP-coupled-anti-GST (Z-5; sc-459, Santa Cruz), mouse-anti-myc (clone 4A6; Millipore), mouse-anti-GFP (B2; Santa Cruz), mouse-anti-Gal4-AD (TA-C10; Santa Cruz), mouse-anti-Gal4-BD (RK5C1; Santa Cruz).

Pulsed-field gel electrophoresis

In the recovery experiments (Fig. 3D, 6B, S3B) $8x10^7$ of cells were taken for every time point and centrifuged at 5,000 x g 10 min at 4 °C. Cells were

resuspended in 1 ml cold 0.1% sodium azide and centrifuged at 3,000 rpm for 3 min. Remaining pellets were resuspended in 50 µl zymolyase buffer (50 mM EDTA, 10 mM Tris pH 8.0, 20 mM NaCl, 1 mg/ml zymolyase (T100)) and mixed with equal amount of 2% agarose. The samples were transferred to the plug mold. The plugs were incubated in zymolyase buffer at 37 °C for 1 h, followed by treatment with proteinase K (0.5 M EDTA pH 8.0, 1 mg/ml proteinase K, 10 mg/ml sodium lauryl sarcosine) at 50 °C for 24-48 h. Next, the plugs were washed 3 times with 50 mM EDTA and loaded. Electrophoresis was performed using the CHEF-DRIII pulsed-field electrophoresis system (Bio-Rad) according to the manufacturer's instructions. The gel was stained with 1 µg/ml ethidium bromide and scanned under UV light. Quantification of PFGE signals was performed using ImageJ. For every time point the signal from the bands that have entered the gel was normalized to the total signal in the lane including that from the well, and the values from every time point were normalized relative to the G1 signal.

2D gel analysis and quantification of replication/recombination intermediates

The experiments were conducted as described previously (Szakal and Branzei, 2013). The DNA samples were digested with HindIII and EcoRV and analysed with probes for ARS305. In all, 200 ml cultures (2-4x10^9 cells) were arrested by addition of sodium azide (final concentration 0.1%) and cooled down in ice. Cells were harvested by centrifugation, washed in cold water, and incubated in spheroplasting buffer (1 M sorbitol, 100 mM EDTA pH 8.0, 0.1% b-ME, and 50 U zymolase/ml) for 1.5 h at 30 °C. In all, 2 ml water, 200

µl RNase A (10 mg/ml), and 2.5 ml Solution I (2% w/v cetyl-trimethyl-ammonium-bromide (CTAB), 1.4 M NaCl, 100 mM Tris-HCl pH 7.6, and 25 mM EDTA pH 8.0) were sequentially added to the spheroplast pellets and samples were incubated for 30 min at 50 °C. In all, 200 µl proteinase K (20 mg/ml) was then added and the incubation was prolonged at 50 °C for 1 h 30 min, and at 30 °C overnight. The sample was then centrifuged at 4,000 rpm for 10 min: the cellular debris pellet was kept for further extraction, while the supernatant was extracted with 2.5 ml chloroform/isoamylalcohol (24/1) and the DNA in the upper phase was precipitated by addition of 2 volumes Solution II (1% w/v CTAB, 50 mM Tris-HCl pH 7.6, and 10 mM EDTA) and centrifugation at 8,500 rpm for 10 min. The pellet was resuspended in 2 ml Solution III (1.4 M NaCl, 10 mM Tris-HCl pH 7.6, and 1 mM EDTA). Residual DNA in the cellular debris pellet was also extracted by resuspension in 2 ml Solution III and incubation at 50 °C for 30 min, followed by extraction in 1 ml chloroform/isoamylalcohol (24/1). The upper phase was pooled together with the main DNA preparation. Total DNA was then precipitated with 1 volume isopropanol, washed with 70% ethanol, air dried, and finally resuspended in TE 1X. Quantification of X-shaped intermediate signals was performed using the Image Quant software as previously described (Liberi et al. 2005; Branzei et al. 2008; Vanoli et al. 2010). For each time point, areas corresponding to the monomer spot (M), the X-spike signal and a region without any replication intermediates as background reference were selected and the signal intensities (SIs) in percentage of each signal were obtained. The values for the X and monomer were corrected by subtracting from the SI value the background value after the latter was multiplied for the ratio between the

dimension of the area for the intermediate of interest and for background. Thus, the values for X and M were calculated in the following way:
Value for X=SI (Xs)-(SI (background) (area (Xs)/area (background));
Value for M=SI (M)-(SI (background) (area (M)/area (background)).
The relative SI for the X was then determined by dividing the value for X with the sum of the total signals (the sum of the X and monomer values). The resulting values for X signals were then normalized. For instance, for recovery experiments the relative value of X obtained after MMS treatment was considered as 100% and the other X values were normalized to it.

Mutation and recombination assays

Mutation rates were determined using a *CAN1* forward mutation assay (Klein 2001). Interchromosomal recombination rates were determined using a direct-repeat system using *leu2* heteroalleles (Aquilera and Klein 1988) and crossover rates were determined using a system harbouring two *arg4* alleles on chromosome V and VIII (Robert et al. 2006, Szakal and Branzei 2013). In all cases mutation/recombination rates were determined using fluctuation analysis and a maximum-likelihood approach. Therefore, for each strain ten independent cultures originated from the single cell were analyzed. To get single colonies 100 cells were plated or streaked out for single colonies on YPD media plates and incubated for 2 days at 30 °C. The frequency of mutants/recombinants in all cultures was determined by plating on selective media. The total cell number was determined by plating an appropriate dilution on non-selective media. For determination of CO rates, for each culture ten ARG+ colonies were picked, analyzed by PCR for CO or NCO

events (Szakal and Branzei 2013) and the overall number of crossover recombinants was extrapolated. From the number of mutants/recombinants/crossover recombinants the number of mutational/recombinational/crossover events was determined using a maximum-likelihood approach and rates were determined by dividing by the number of cell divisions (Pfander et al. 2005). For each strain 2-10 independent experiments were performed to determine mean and standard deviation.

Microscopy and immunofluorescence

Yeast cells were grown in synthetic complete (SC) medium supplemented with 100 µg/ml adenine (SC+Ade) and processed for fluorescence microscopy as described (Eckert-Boulet et al. 2011). For staining of DNA in live yeast cells, 5 µg/ml of Hoechst 33258 (B2883, Sigma-Aldrich) were added to the culture 10-15 min prior to microscopy and washed out with fresh medium immediately prior to microscopy and imaged at 25 °C. Fluorophores used in yeast were cyan fluorescent protein (CFP, clone W7) (Heim and Tsien 1996) and yellow fluorescent protein (YFP, clone 10C) (Ormo et al. 1996). Microscopy was performed using an AxioImager Z1 (Carl Zeiss MicroImaging, Inc) equipped with a 100x objective lens (Zeiss PLAN-APO, NA 1.4), a cooled Orca-ER CCD camera (Hamamatsu, Japan), differential interference contrast (DIC), and a Zeiss HXP120C illumination source, or on a Deltavision Elite microscope (Applied Precision, Inc) equipped with a 100x objective lens (Olympus U-PLAN S-APO, NA 1.4), a cooled Evolve 512 EMCCD camera (Photometrics, Japan), and a Insight solid state illumination source (Applied

Precision, Inc). Images were acquired using Volocity (PerkinElmer) or softWoRx (Applied Precision, Inc) software. Images were acquired and processed using Volocity (PerkinElmer) software. Images were pseudocoloured according to the approximate emission wavelength of the fluorophores.

For analysis of RPA foci (Fig. 3F) cells were grown in SC media, arrested with α-factor and treated in S-phase with 0.033% MMS for 120 min, then released into the fresh SC media for recovery. For microscopy cells were fixed in FA for 30 min and quenched in 2.5 M glycine for 30 min. Cells were washed twice and resuspended in 50 mM Tris, pH 7.5. Images of cells were obtained using a fully automated Zeiss inverted microscope (AxioObserver Z1) equipped with a MS-2000 stage (Applied Scientific Instrumentation, USA), a CSU-X1 spinning disk confocal head (Yokogawa, Herrsching), LaserStack Launch with selectable laser lines (Intelligent Imaging Innovations, USA) and an X-CITE Fluorescent Illumination System. Images were captured using a CoolSnap HQ camera (Roper Scientific, Canada) under the control of the Slidebook software (Intelligent Imaging Innovations, USA). All fluorescence signals were imaged with a 63x oil objective.

Cell culture and transfection techniques

HEK 293T cells were cultured at 37 °C at 7.5% CO_2 in DMEM (GIBCO-BRL) supplemented with 10% FCS. Transient transfections were performed in 6-well plates (HeLa) using the calcium phosphate method. In general $5x10^5$ 293T cells per well were seeded and transfected the next day using 20 µg

total DNA. After 4-6 h incubation the TF medium was replaced with fresh growth medium, and cells were cultured for another 18-20 h.

Nuclease assays

5'-end-Cy3-labeled oligonucletides were used to prepare synthetic DNA substrates as described (Rass & West 2006). Nuclease assays were carried out with immobilized Mms4-FLAG. The Anti-FLAG immunoprecipitates were extensively washed and mixed with 10 µl reaction buffer (50 mM Tris-HCl pH 7.5, 3 mM $MgCl_2$) containing ~2.5 nM 5'-Cy3-end-labeled substrate (Matos et al 2011). Reactions were incubated for 15-45 min with gentle rotation at 30 °C and stopped by addition of 4 µl 10 mg/ml proteinase K and 2% SDS, and further incubation at 37 ºC for 1 h. Loading buffer was added and radiolabeled products were separated by 10% PAGE, and analyzed using a Typhoon scanner.

Sequence analysis

Close orthologues of budding yeast and human Slx4 were found by NCBI-BLAST (Altschul et al. 1997) and verified by reciprocal BLAST searches. Individual multiple sequence alignments of fungal and mammalian Slx4 were done using ClustalX (Chenna et al. 2003). The Profile Alignment feature was used in ClustalX to align the two profiles from mammalian and fungal Slx4 proteins. This identified the potential Dpb11/TopBP1 interaction motif in human Slx4. Slx4 proteins from further classes were identified by BLAST and first aligned with members of their individual class using ClustalX. Resulting multiple sequence alignments were manually analyzed for the occurrence of

the Dpb11/TopBP1 motif and subsequently manually aligned to the yeast and mammalian motif.

Species abbreviations and accession numbers for Figure S2.

Sp	Schizosaccharomyces pombe	NP_594064
Sc	Saccharomyces cerevisiae	NP_013236
Kl	Kluyveromyces lactis	XP_453790
Ec	Eremothecium cymbalariae	XP_003646141
Nc	Naumovozyma castellii	XP_003928518
Ka	Kazachstania naganashii	CCK71307 (emb)
Td	Toluraspora delbrueckii	XP_003682477
Zr	Zygosaccharomyces rouxii	XP_002497655
Vp	Vanderwaltozyma polyspora	XP_001647185
Lt	Lachancea thermotolerans	XP_002555561
Hs	Homo sapiens	NP_115820
Sb	Samiri b. boliviensis	XP_003928518
Mm	Mus musculus	NP_803423
Rn	Rattus norvegicus	XP_001079342
Sh	Sacrophilus harrisii	XP_003761955
Tm	Trichechus manatus latirostris	XP_004373478
Oo	Orcinus orca	XP_004270504
Xt	Xenopus tropicalis	XP_002932505
Dr	Danio rerio	XP_003201146
Dm	Drosophila melanogaster	NP_648104
Dg	Drosophila grimshawi	XP_001983575
Dw	Drosophila willistoni	XP_002062409
Cc	Ceratitis capitata	XP_004526156
Ag	Anopheles gambiae	XP_001687887

References

Aguilera A, Klein HL. (1988). Genetic control of intrachromosomal recombination in Saccharomyces cerevisiae. I. Isolation and genetic characterization of hyper-recombination mutations. Genetics. 119, 779-790.

Altschul SF, Madden TL, Schäffer AA, Zhang J, Zhang Z, Miller W, Lipman DJ. (1997). Gapped BLAST and PSI-BLAST: a new generation of protein database search programs. Nucleic Acids Res. 25, 3389-3402.

Branzei D, Vanoli F, Foiani M. (2008). SUMOylation regulates Rad18-mediated template switch. Nature. 7224, 915-920.

Chenna R, Sugawara H, Koike T, Lopez R, Gibson TJ, Higgins DG, Thompson JD. (2003). Multiple sequence alignment with the Clustal series of programs. Nucleic Acids Res. 31, 3497-3500.

Cox J, Mann M. (2008). MaxQuant enables high peptide identification rates, individualized p.p.b.-range mass accuracies and proteome-wide protein quantification. Nat Biotechnol. 26, 1367-1372.

Eckert-Boulet N, Rothstein R, Lisby M. (2011). Cell biology of homologous recombination in yeast. Methods Mol Biol. 745, 523-536.

Gonzalez-Huici V, Szakal B, Urulangodi M, Psakhye I, Castellucci F, Menolfi D, Rajakumara E, Fumasoni M, Bermejo R, Jentsch S, Branzei D. (2014).

DNA bending facilitates the error-free DNA damage tolerance pathway and upholds genome integrity. EMBO J. (Epub ahead of print).

Heim R, Tsien RY. (1996). Engineering green fluorescent protein for improved brightness, longer wavelengths and fluorescence resonance energy transfer. Curr Biol. 6, 178-182.

James P, Halladay J, Craig EA. (1996). Genomic libraries and a host strain designed for highly efficient two-hybrid selection in yeast. Genetics. 144, 1425-1436.

Klein HL. (2001). Mutations in recombinational repair and in checkpoint control genes suppress the lethal combination of srs2Delta with other DNA repair genes in Saccharomyces cerevisiae. Genetics. 157, 557-565.

Knop M, Siegers K, Pereira G, Zachariae W, Winsor B, Nasmyth K, Schiebel E. (1999). Epitope tagging of yeast genes using a PCR-based strategy: more tags and improved practical routines. Yeast. 15, 963-972.

Liberi G, Maffioletti G, Lucca C, Chiolo I, Baryshnikova A, Cotta-Ramusino C, Lopes M, Pellicioli A, Haber JE, Foiani M. (2005). Rad51-dependent DNA structures accumulate at damaged replication forks in sgs1 mutants defective in the yeast ortholog of BLM RecQ helicase. Genes Dev. 19, 339-350.

Matos J, Blanco MG, Maslen S, Skehel JM, West SC (2011) Regulatory control of the resolution of DNA recombination intermediates during meiosis and mitosis. Cell 147**:** 158-172

Mullen JR, Kaliraman V, Ibrahim SS, Brill SJ. (2001). Requirement for three novel protein complexes in the absence of the Sgs1 DNA helicase in Saccharomyces cerevisiae. Genetics. 157, 103-118.

Ormö M, Cubitt AB, Kallio K, Gross LA, Tsien RY, Remington SJ. (1996). Crystal structure of the Aequorea victoria green fluorescent protein. Science. 273, 1392-1395.

Pfander B, Moldovan GL, Sacher M, Hoege C, Jentsch S. (2005). SUMO-modified PCNA recruits Srs2 to prevent recombination during S phase. Nature. 7049, 428-433.

Rass U, West SC (2006) Synthetic junctions as tools to identify and characterise Holliday junction resolvases. In *Meth. Enzymol.*, Campbell JL, Modrich P (eds), Vol. 408, pp 485-501. San Diego: Elsevier

Robert T, Dervins D, Fabre F, Gangloff S. (2006). Mrc1 and Srs2 are major actors in the regulation of spontaneous crossover. EMBO J. 25, 2837-2846.

Szakal B, Branzei D. (2013). Premature Cdk1/Cdc5/Mus81 pathway activation induces aberrant replication and deleterious crossover. EMBO J. 32, 1155-1167.

Thomas BJ, Rothstein R. (1989). Elevated recombination rates in transcriptionally active DNA. Cell. 56, 619-630.

Vanoli F, Fumasoni M, Szakal B, Maloisel L, Branzei D. (2010). Replication and recombination factors contributing to recombination-dependent bypass of DNA lesions by template switch. PLoS Genet. 6: e1001205.